



Contents lists available at ScienceDirect

# Opto-Electronics Review

journal homepage: <http://www.journals.elsevier.com/pto-electronics-review>

## Review

# Ion etching of HgCdTe: Properties, patterns and use as a method for defect studies<sup>☆</sup>

I.I. Izhnin<sup>a,b</sup>, K.D. Mynbaev<sup>c,d,\*</sup>, A.V. Voitsekhovskii<sup>b</sup>, A.G. Korotaev<sup>b</sup>, O.I. Fitsych<sup>e</sup>,  
M. Pociask-Bialy<sup>f</sup>

<sup>a</sup> Scientific Research Company "Carat", Lviv 79031, Ukraine

<sup>b</sup> National Research Tomsk State University, Tomsk 634050, Russia

<sup>c</sup> Ioffe Institute, St.-Petersburg 194021, Russia

<sup>d</sup> ITMO University, St.-Petersburg 197101, Russia

<sup>e</sup> P. Sahaydachnyi National Army Academy, Lviv 79012, Ukraine

<sup>f</sup> Center for Microelectronics and Nanotechnology of the University of Rzeszow, Rzeszow 35-310, Poland

## ARTICLE INFO

### Article history:

Received 16 January 2017

Accepted 28 March 2017

Available online 29 April 2017

This review is dedicated to the memory of our friend and colleague Prof. V.V. Bogoboyashchyy.

### Keywords:

HgCdTe  
Ion etching  
Photodetectors  
Defects  
Doping

## ABSTRACT

Analysis is performed of the contemporary views on the effect of ion etching (ion-beam milling and reactive ion etching) on physical properties of HgCdTe and on the mechanisms of the processes responsible for modification of these properties under the etching. Possibilities are discussed that ion etching opens for defect studies in HgCdTe, including detecting electrically neutral tellurium nanocomplexes, determining background donor concentration in the material of various origins, and understanding the mechanism of arsenic incorporation in molecular-beam epitaxy-grown films.

© 2017 Association of Polish Electrical Engineers (SEP). Published by Elsevier B.V. All rights reserved.

## 1. Introduction

Hg<sub>1-x</sub>Cd<sub>x</sub>Te (MCT) solid solutions, since they were synthesized for the first time at Royal Radar Establishment (UK) and Lviv State Pedagogical Institute (USSR) in the middle of the last century [1,2], have remained the basic material for the fabrication of highly effective photodetectors operating in the infrared (IR) part of the spectrum (2.5–20 μm) [3]. This status of MCT is pre-defined by the electronic structure of this material and is expected to remain such for at least two decades more.

In MCT technology, methods of 'dry etching', including ion-beam milling or reactive ion etching, are used quite widely. These processing techniques are based on the irradiation of the surface of the

material with low-energy (0.2–2 keV) ions of noble gases (mostly Ar) or mixture of Ar with chemically active gases (H<sub>2</sub>, CH<sub>4</sub>). Initially, such etching was used for dry cleaning and sputtering of the material with the aim of formation of specific surface topology and/or contact areas of sensitive elements of photodetectors [4–6]. Later, ion etching was used to form the topology of MCT-based matrix-type mesa-diodes, including multi-color ones [7–9]. The results of the use of various types of dry etching in application to MCT etching in a sense of sputtering (material removal) were reviewed in Ref. [10], yet the effect of such treatment on *physical* properties of MCT in that paper was not considered.

In 1981, in a patent by Wotherspoon [11] it was declared, for the first time, that ion etching of vacancy-doped *p*-MCT (where conductivity type was defined by intrinsic acceptors, mercury vacancies V<sub>Hg</sub>) led to *p*-to-*n* conductivity type conversion (CTC). This effect was proposed as a tool for fabrication of *p*-*n* junctions of photodiodes. Wide-scale studies of the effect of ion etching on the properties of MCT began after 1990, and at that time, this method also was introduced into industrial production of photodiodes. As the properties of MCT change in a similar way under both ion

<sup>☆</sup> This article is an expanded version of the scientific reports presented at the International Conference on Semiconductor Nanostructures for Optoelectronics and Biosensors 2016 ICSeNOB2016, May 22–25, 2016, Rzeszow, Poland.

\* Corresponding author at: Ioffe Institute, St.-Petersburg 194021, Russia.

E-mail addresses: [i.izhnin@carat.electron.ua](mailto:i.izhnin@carat.electron.ua) (I.I. Izhnin), [mynkad@mail.ioffe.ru](mailto:mynkad@mail.ioffe.ru) (K.D. Mynbaev).

## List of abbreviations and symbols used throughout the text

### Abbreviations

AO	anodic oxide
CTC	conductivity type conversion
DC	direct current
EBIC	electron beam induced current
IE	ion etching
ISOVPE	isothermal vapor-phase epitaxy
LBIC	laser-beam induced current
LPE	liquid phase epitaxy
MBE	molecular beam epitaxy
MCT	mercury cadmium telluride, $Hg_{1-x}Cd_xTe$
MOCVD	metal-organic chemical vapor deposition
MSA	mobility spectrum analysis
RF	radio frequency
SIMS	secondary-ion mass-spectroscopy
VPE	vapor-phase epitaxy
WBPL	wide-bandgap protective layer

### Symbols

$a$	HgCdTe lattice parameter
$B$	magnetic field
$C_{v0}$	initial concentration of mercury vacancies in the damaged area
$C_{w0}$	initial concentration of mercury bivacancies in the damaged area
$d_j$	conductivity type conversion depth
$d_r$	conductivity type conversion depth reduced to mercury vacancy concentration
$D$	ion dose
$D_I$	mercury interstitial diffusion coefficient
$D_V$	mercury vacancy diffusion coefficient
$E_C$	energy of the conduction band
$E_F$	Fermi energy
$E_g$	energy gap
$E_M$	energy of mercury interstitial migration
$E_V$	energy of the valence band
$E$	ion energy
$e$	elementary charge
$\mathbf{J}(J_{Hg})$	mercury flux
$j$	ion current density
$Hg_I$	interstitial mercury
$[Hg_I]_s$	concentration of $Hg_I$ in the diffusion source under ion etching
$k_B$	the Boltzmann constant
$K_F$	equilibrium constant for the reaction between mercury vacancy and interstitial
$k_F$	reaction rate constant between mercury vacancy and interstitial
$k_w$	reaction rate constant between mercury bivacancy and interstitial
$K_{rM}$	equilibrium constant for the reaction between interstitial mercury and I-group acceptor
$K_X$	equilibrium constant for the reaction between interstitial mercury and arsenic atom
$L_d$	defect layer thickness, radius of defect zone
$L_y$	protective layer thickness
$l_0$	a factor
$N_0$	node density in crystal (sub)lattice
$N_A$	acceptor concentration
$N_{As}$	arsenic concentration
$N_{BD}$	background donor concentration

$N_D$	donor concentration
$N_A - N_D$	( $N_D - N_A$ ) concentration of uncompensated acceptors (donors)
$N_{In}$	indium concentration
$N_{tr}$	density of capture centers for mercury interstitials
$n$	electron concentration
$n_{77i}$	electron concentration measured straight after ion etching
$n_{77f}$	electron concentration measured after relaxation
$n_{77(0)}$	electron concentration measured before ion etching
$n_i$	intrinsic carrier concentration
$p_{77}$	hole concentration measured at 77 K
$R(\mathbf{r}, t)$	rate of mercury interstitial capture on radiation-induced defects
$R_H$	the Hall coefficient
$R_p$	projected ion path
$r_F$	mercury interstitial caption radius on a mercury vacancy
$r_w$	mercury interstitial caption radius on a mercury bivacancy
$r_0$	screening length (radius)
$S$	effective cross-section of the defect formation zone
$S_I$	a function describing $Hg_I$ source
$T$	temperature
$T_{cr}$	temperature of the cracker cell in MBE of MCT
$T_{src}$	temperature of the arsenic source in MBE of As-doped material
$T_s$	sample temperature during ion etching
$T_{sb}$	substrate temperature during MCT growth
$t$	time
$V_{Hg}$	mercury vacancy
$W_{Hg}^x$	neutral mercury bivacancy
$x$	alloy composition (CdTe molar fraction in $Hg_{1-x}Cd_xTe$ )
$x_a$	alloy composition in the active layer of heteroepitaxial HgCdTe structure
$x_j d_j$	conversion depth
$x_{y,y}$	composition at the surface of graded-gap wide-bandgap protective layer
$z$	co-ordinate axis normal to crystal surface
$\delta_0$	mercury deficiency
$\varepsilon$	dielectric constant
$\Delta H_{cx}$	enthalpy of the formation of the complex of interstitial mercury with arsenic
$\Delta L_0$	thickness of the defect layer that acts as a mercury source
$\mu_{n77}, \mu_{p77}$	carrier mobility measured at 77 K
$\sigma$	conductivity
$\varphi$	electric potential
$\Phi$	ion fluence
$\tau$	non-equilibrium carrier lifetime

milling and reactive ion etching, we shall further refer to both kinds of treatment as to 'ion etching' (IE). Also, as the main patterns of the changes in the properties of MCT under IE are valid for the material with *p*- and *n*-type, we shall often speak of 'modification' of these properties.

Some aspects of the effect of IE on the properties of MCT were reviewed by Ivanov-Omskii and Mynbaev in 2002 [12]. At that point, it looked like that the development of the technology was far ahead of understanding of physical processes that occurred under IE. In the last 15 years this understanding has demonstrated a substantial progress. In particular, the effect of IE on the properties of

MCT films with wide-bandgap protective surface layers grown with molecular beam epitaxy (MBE) and metal-organic chemical vapour deposition (MOCVD) on various substrates, including those made of GaAs and Si, was studied in detail. The properties of ion-etched MCT doped with I- and V-group acceptors were studied. Also, detailed studies of the relaxation of electrical parameters of ion-etched MCT were performed. A considerable progress was achieved in relation to understanding the structure of a radiation-damaged layer, which inevitably forms at the surface of the material treated with energetic ions, as well as in relation to the effect of this layer on the properties of the converted/modified ‘bulk’ layer. All this knowledge allowed for building a complete and a self-aligned pattern, which described modification of the properties of MCT during and after IE. Quantitative models were developed that described the processes responsible for CTC. These included: the mechanism of the formation of the source of interstitial mercury responsible for CTC, the nature of compositional dependence of CTC depth, mechanisms of CTC in vacancy-doped and I- and V-group acceptor-doped *p*-type material, mechanisms of relaxation of electrical parameters of MCT after IE, etc. Some of these issues were partly addressed by Shaw and Capper in Refs. [13,14].

Analysis of the properties of MCT subjected to IE allowed the authors of this review to conclude that IE can be used as an effective method for studying defects in MCT. This fact was first pointed out to in Ref. [15]. Later, IE was used for the study of defects in MCT samples of various origin, e.g., for the investigation of neutral defects in MCT grown with MBE and liquid-phase epitaxy (LPE), for the study of background donor doping in MCT, for the study of the mechanisms of arsenic incorporation during MBE, etc. Thus, the task of this review is to analyze the current views on the effect of IE on the properties of MCT and on the mechanisms of the physical processes responsible for the modification of MCT under IE, as well as to discuss possibilities, which IE opens for defect studies.

## 2. Properties of ion-etched MCT and patterns of its modification

As mentioned above, the effect of CTC in vacancy-doped MCT under IE was discovered by Wotherspoon [11]. Further studies revealed that deep CTC under IE was typical only of MCT and some other Hg-containing narrow-gap semiconductors ( $Hg_{1-x}Mn_xTe$ ,  $Hg_xZn_{1-x}Te$ ) [12,16,17], and could not be observed in InSb (with electronic structure similar to that in MCT) or PbSnTe (with energy gap values close to those in MCT) [18,19]. Also, *p*-to-*n* CTC (or modification of parameters) was observed in MCT grown with all known synthesis methods: bulk crystals grown from melts [11,20–28] and

with solid-state re-crystallization [29], epitaxial films grown with LPE [30–33], vapour-phase epitaxy (VPE) [16], MOCVD [34] and MBE [35–37]. Thus, it became clear that the effect of CTC under IE is not related to a particular growth technology, but rather was an inherent property of MCT and related materials.

To explain CTC in vacancy-doped MCT, from the very beginning it was suggested that conversion was caused by fast migration of atoms of interstitial mercury  $Hg_I$ , generated on (or close to) the surface (these intrinsic defects are the most mobile in MCT). This thesis has been accepted by all the community [12]. However, the early CTC model, which implied over-compensation of intrinsic acceptors  $V_{Hg}$  by  $Hg_I$  [11], was later rejected, and presently, it is of common belief that in vacancy-doped MCT the CTC is due to mutual annihilation of  $V_{Hg}$  and  $Hg_I$  with resulting *n*-type conductivity being defined by residual donors. Below we shall consider basic properties and regularities of CTC in MCT under IE.

### 2.1. Propagation of a conductivity type conversion front under ion etching

For understanding the processes responsible for CTC in MCT under IE it was important to study the propagation of the conversion front, i.e., the dependence of conversion depth  $d_j$  on IE time  $t$  (or ion fluence  $\Phi = j \cdot t/e$ , where  $j$  is ion current density and  $e$  is the elementary charge), sample temperature  $T_s$  and material parameters (concentration of uncompensated acceptors  $N_A - N_D$ , composition  $x$ ). Under typical IE conditions (ion energy  $E < 2$  keV,  $j < 1$  mA/cm<sup>2</sup> and  $t \sim 10$ –30 min),  $d_j$  could achieve tens and even hundreds of micrometers (see, e.g., [11,24–26,31]). These depths exceeded the projected ion path  $R_p$  (of the order of 2–3 nm) by 4 to 5 orders of magnitude (for comparison, under ion implantation, where ion energy is of the order of hundreds of keV,  $d_j/R_p \sim 10$ ). Also, they greatly exceeded CTC depths achievable under thermal annealing in mercury vapours (and typical IE is performed at 300 K), which was indicative of extremely high rate of CTC front propagation and required an explanation.

The  $d_j(t)$  data available in the literature are summarized in Fig. 1. To describe the CTC front propagation, two different models were developed. The first one (historically) was a kinetic model, which assumed that  $d_j(t) \sim t/(N_A - N_D)$  (i.e., it gave linear relation  $d_j(t)$ ), and was based on the belief that the CTC front velocity was defined by the rate of generation of  $Hg_I$  at/close to the MCT surface as a result of material sputtering (curve 3). This concept was developed by the authors of Refs. [11,21], and later, Refs. [38,39]. In particular, in Refs. [11,21]  $d_j \sim t^{0.85}$ , and thus,  $d_j(t)$  was close to linear dependence. This relation was obtained for *p*-MCT bulk crystals ( $x \sim 0.2$ ,  $N_A - N_D = 10^{16}$  cm<sup>-3</sup>) ion-etched with  $j = 0.6$  mA/cm<sup>2</sup> and  $E = 500$  eV. CTC depth in these experiments reached  $\sim 200$   $\mu$ m for  $t = 60$  min.

The second model is a diffusion one and it assumes  $d_j(t) \sim \sqrt{t/(N_A - N_D)}$ . The CTC front rate in this case is limited by  $Hg_I$  concentration in a sub-surface source, which forms under IE (curves 1, 2 and 4). This concept was introduced in Refs. [24,25,32] and later was developed in Refs. [40,41]. For example, detailed studies of  $d_j(t)$  in MCT etched with neutralized Ar ions ( $j = 0.06$ –0.30 mA/cm<sup>2</sup>,  $E = 1200$ –1800 eV, no sample cooling) were performed on LPE-grown *p*-MCT films ( $N_A - N_D = 5 \times 10^{15}$ – $4 \times 10^{17}$  cm<sup>-3</sup>,  $x \approx 0.2$ ) (Fig. 1, curve 4) [31,32], and the results confirmed  $d_j(t) \sim \sqrt{t/(N_A - N_D)}$  relation. The dependence  $d_j(t) \sim \sqrt{t}$  was also observed in Ref. [24], when *p*-MCT bulk crystals ( $N_A - N_D = 10^{16}$ – $5 \times 10^{16}$  cm<sup>-3</sup>,  $x = 0.20$ –0.23) were subjected to IE with neutralized Ar ions ( $j = 0.6$  mA/cm<sup>2</sup>,  $E = 750$  eV,  $T_s \approx 50$  °C). Conversion depths 40–385  $\mu$ m were achieved for  $t = 10$ –30 min (Fig. 1, curve 2). A similar relation ( $d_j(t) \sim \sqrt{t}$ ) was obtained by the same authors during reactive IE of bulk

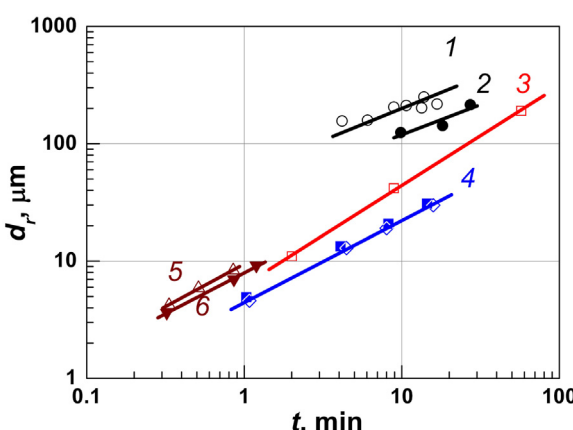


Fig. 1. Dependences of the conversion depth  $d_j$  (reduced to typical value  $N_A - N_D = 10^{16}$  cm<sup>-3</sup>) on IE time: curve 1, [25]; 2, [24]; 3, [11]; 4, [32]; 5, 6, [35,36].

p-MCT ( $N_A = N_D = 10^{16} \text{ cm}^{-3}$ ,  $x = 0.21$ ) in radio-frequency (RF,  $f = 13.56 \text{ MHz}$ )  $\text{H}_2/\text{CH}_4$  plasma (discharge power 180 W, bias 300 V,  $T_s \approx 40^\circ\text{C}$ ) (Fig. 1, curve 1) [25].

Detailed studies of  $d_j(t)$  were reported on in Refs. [35,36], where MBE-grown ((211)B CdZnTe substrate) p-MCT structures with surface wide-bandgap protective layers (WBPL) were subjected to IE (Fig. 1, curves 5 and 6). The composition of the ‘active’ layer (the one with constant  $x$ )  $x_a$  in the structures was 0.21, 0.23 or 0.31. 15 min after the growth of the ‘active’ layer, a protective CdTe layer was deposited *in situ*. As the deposition of CdTe layers was performed in residual Hg atmosphere, in reality these layers represented  $\text{Hg}_{1-y}\text{Cd}_y\text{Te}$  with big  $y$  values. Hole-type conductivity ( $N_A - N_D = 10^{16} - 10^{17} \text{ cm}^{-3}$ ) of the structures was achieved by annealing in vacuum at  $T = 250^\circ\text{C}$  (1.5 h) or  $T = 325^\circ\text{C}$  (24 h). Obviously, the composition of the surface layer changed as a result of the annealing, but this was difficult to follow. The structures were subjected to IE with  $\text{Ar}^+$  ions ( $E = 700 \text{ eV}$ ) with  $j = 0.14$  or  $0.54 \text{ mA/cm}^2$  and  $t = 16 - 650 \text{ s}$  with sample cooling with water. CTC depth was measured with electron beam induced current (EBIC). In Ref. [35], the authors claimed that linear  $d_j(t)$  dependence was observed for  $d_j < 4 \mu\text{m}$ , while for larger depths  $d_j$  was proportional to  $\sqrt{t}$ . In Ref. [36], basing on the analysis performed on the same group of samples, the authors claimed that at  $d_j < 10 \mu\text{m}$   $d_j$  depended on  $t$  linearly. As will be shown below, this was in fact the influence of the WBPL.

An important point that should be addressed by any model is the reason for extremely high migration rate of  $\text{Hg}_I$  under typical IE condition, when the sample is kept at the temperature close to 300 K (or even lower). Peculiarities of chemical diffusion of Hg in MCT under annealing in mercury vapours are well-known [42]. At  $T < 420^\circ\text{C}$  metal vacancies are virtually unmovable and maintain local equilibrium with  $\text{Hg}_I$ , thus a mass action law is valid,  $[V_{\text{Hg}}] \cdot [\text{Hg}_I] = K_F$ , where square brackets stand for concentration,  $K_F$  is equilibrium constant. The dependence of CTC depth on IE time is defined as follows:  $d_j = \sqrt{2D_I \cdot t \cdot [\text{Hg}_I]_S / [V_{\text{Hg}}]}$ , where  $D_I$  is the diffusion coefficient of  $\text{Hg}_I$ , and  $[\text{Hg}_I]_S$  is the concentration of  $\text{Hg}_I$  in the diffusion source. Therefore, the rate of CTC front is strongly affected by the value of  $[\text{Hg}_I]_S$ . Shaw and Capper [43] made estimations of  $[\text{Hg}_I]_S$  for various conversion methods that related to diffusion model (thermal annealing in mercury vapors, annealing of anodic oxide, IE). In particular, for IE data presented in Refs. [24] and [32],  $[\text{Hg}_I]_S$  was found to equal  $2.9 \times 10^{13}$  and  $2.4 \times 10^{14} \text{ cm}^{-3}$ , respectively. These values were 7 to 8 orders of magnitude higher than  $[\text{Hg}_I]_S$  in saturated mercury vapours at temperatures typical of IE and could indeed provide huge acceleration of CTC front under the etching. So, the main problem was to explain the mechanism of the formation of mercury source with such high  $[\text{Hg}_I]_S$ . This problem was solved by the authors of Refs. [40,41,44].

Let us note some more features of CTC in MCT under IE. The authors of Ref. [27] studied the effect of  $T_s$  on the  $d_j$  value. In their experiments, a cooling system embedded in the IE machine kept  $T_s$  at 100, 130, 170, 230, or 330 K. The CTC depth was measured using EBIC. It was found that CTC was a temperature-stimulated process, and  $d_j$  decreased exponentially with temperature decreasing. No CTC was observed at  $T < 100 \text{ K}$ . The authors of Ref. [27] concluded that such  $d_j(T)$  dependence was due to that of  $D_I$  on  $T$  according to the Arrhenius law:

$$D_I = D_0 \exp(-E_M/k_B T), \quad (1)$$

where  $E_M$  is the energy of  $\text{Hg}_I$  migration. Within the frames of this approach, they found from their experimental  $d_j(T)$  data that  $E_M$  was equal to  $\sim 0.12 \text{ eV}$ . This value agreed well with estimations of the energy of migration of  $\text{Hg}_I$  performed *ab initio* in Ref. [45], which validated CTC diffusion model.

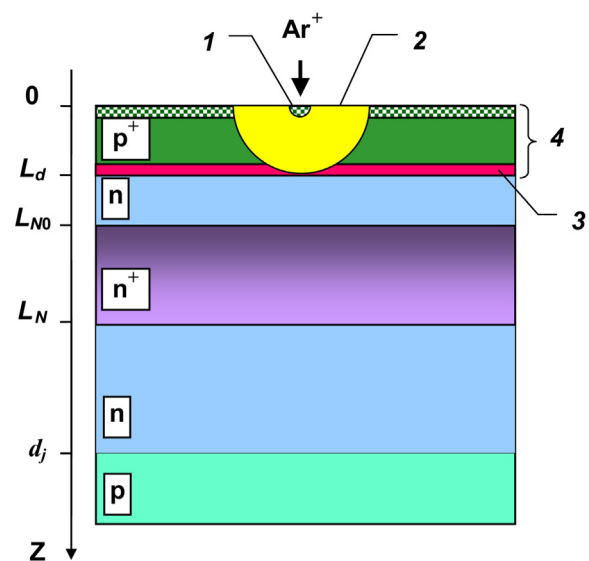


**Fig. 2.** Schematics of  $p$ - $n$  junction formed in MCT under IE (proportion between the thicknesses of the layers is not observed): 1, etching zone; 2, defect formation zone; 3, Hg<sub>I</sub> source; 4, defect layer (after [41]).

Also, a fact of lateral extension of CTC front was established in Refs. [24,35] using EBIC. In these experiments, a photoresist mask was used, which protected a part of each sample from energetic ions. In Ref. [24], a  $\sim 80 \mu\text{m}$ -wide lateral propagation of CTC was established with vertical  $d_j$  being  $170 \mu\text{m}$ . The authors of Ref. [35] concluded, on the basis of the results of a number of experiments, that lateral CTC depth followed  $\sim 0.5d_j$ . These results also confirmed the validity of the diffusion model.

The authors of Ref. [33] established that CTC depth in LPE-grown MCT films decreased with  $x$  increasing in the  $x$  range 0.29–0.39. For MCT with  $x \geq 0.4$  the depth was lower than  $0.5 \mu\text{m}$ . In Ref. [41], a similar conclusion was made on the basis of the results of IE of  $p$ -MCT bulk crystals with  $x = 0.16 - 0.30$ . However, in Ref. [38] the authors reported on the observation of deep (up to  $40 \mu\text{m}$ ) CTC in vacancy-doped LPE-grown  $p$ -MCT with  $x = 0.45$  after electron cyclotron resonance etching, which removed  $\sim 3 \mu\text{m}$  of surface layer. The nature of compositional dependence of CTC depth in MCT under IE was proposed by the authors of Ref. [41] and will be considered below.

An alternative explanation for very fast migration of  $\text{Hg}_I$  under IE was given by the authors of Ref. [29], who suggested that the reason for that was the excitation of metal sublattice with the ion beam. This assumes that CTC depth should not depend on  $T_s$ , which contradicts experimental data [27]. Thus, there has been no consensus on whether  $d_j$  actually should depend on IE time linearly or as  $d_j(t) \sim \sqrt{t}$ .

## 2.2. Mechanism of the formation of the interstitial mercury source

The  $\text{Hg}_I$  source is a very important point. As the primary effect of IE is the interaction of energetic ions with the surface of the material and sputtering of the surface layer, the kinetic model assumes that  $\text{Hg}_I$  source is the etched-off MCT layer. For example, in Ref. [38] it was stated that one  $\text{Hg}_I$  atom is produced during the etch process for each 48,000 atoms removed from the surface for MCT with  $x \sim 0.3$  and one  $\text{Hg}_I$  is produced for each 144,000 atoms removed for  $x \sim 0.4$ .

A different model of the formation of the  $\text{Hg}_I$  source was developed by the authors of Refs. [40,41,44]. Fig. 2 shows schematics of  $p$ - $n$  junction formed in MCT under IE according to Ref. [41]. According to Ref. [46], MCT etching with ions with  $\sim 1 \text{ keV}$  energy sputters

only 2–3 atomic surface layers (etching zone 1 in Fig. 2). The most part of the ion energy transforms into thermal energy in the zone of a so called ‘thermal spike’. Inside the spike the crystal lattice gets destroyed, but due to quick scattering of the excessive energy, the spike cools down very quickly and the lattice is partly restored. On the other hand, the energy  $E \approx 0.5$  keV is enough to form two hundred pairs of  $\text{Hg}_l^+$  and  $V_{\text{Hg}}^+$  (Frenkel’s pairs), as each of them requires about 2.3 eV in MCT with  $x \sim 0.2$  [47]. The energy of the formation of Te-related point defects is much higher, thus the probability of the appearance of these defects is much lower. Because of that, one can assume that the close order in anion sublattice under IE is still maintained. Assuming that part of the energy of the ion spent on defect formation is comparable with that spent on heating, it can be assessed that in MCT crystal around each point where an ion with  $E \approx 0.5$  keV hits the lattice, a nano-sized ‘hot’ zone is formed with the radius of  $L_d \sim 5$  nm (defect zone 2 in Fig. 2). On the periphery of this zone, cation sublattice defects dominate, including doubly charged  $\text{Hg}_l^{++}$  and  $V_{\text{Hg}}^{++}$ , whose initial concentration approaches  $10^{21} \text{ cm}^{-3}$ .

As the probability of finding a vacant site is quite large ( $\sim 0.1$ ), some of  $V_{\text{Hg}}^{++}$  form non-equilibrium neutral complexes, mercury bivacancies  $W_{\text{Hg}}^x$ , and their concentration  $C_{\text{W0}}$  approaches  $2.5 \times 10^{20} \text{ cm}^{-3}$ . Due to the small size of defect formation zone ( $L_d \sim 5$  nm), the damaged area cools down at  $\sim 10^{-12}$  s, and this time is comparable with the minimum period of lattice vibration. Thus, after cooling down, this area generally retains the initial defect structure. As the spike cools down very quickly, defects do not have time to migrate much further than the distance equal to lattice constant. Thus, diffusion processes that occur in the thermal spike at high temperatures can be neglected. Therefore, the process of accumulation of excessive mercury is related to the diffusion of non-equilibrium  $\text{Hg}_l^+$  from the area of the cooled spike. During the short period of the cooling of the spike ( $t < 10^{-12}$  s) the system of Frenkel’s defects does not reach the equilibrium, and in the cooled zone there remains a lot of defects, which relax via mutual annihilation, while mobile  $\text{Hg}_l^+$  atoms have a chance to penetrate into the bulk of the material.

Due to mercury atoms moving from the area of defect formation into the crystal, as well as to preferential mercury evaporation during IE [46], a substantial mercury deficiency occurs in a thin surface defect layer with the thickness of  $L_d$  (Fig. 2). This was experimentally confirmed with X-ray photoelectron spectroscopy [7]. Total mercury deficiency  $\delta_0$  in the defect layer is determined by the condition of its total non-transparency to  $\text{Hg}_l^+$  and equals  $\delta_0 \sim 10^{19} \text{ cm}^{-3}$  [41]. Kinetics of the relaxation of major defects of the cation sublattice in the cooled area of the spike,  $[V_{\text{Hg}}^+]$ ,  $[\text{Hg}_l^+]$  and  $[W_{\text{Hg}}^x]$  can be described by the following system of equations:

$$\left. \begin{aligned} \frac{d}{dt} [V_{\text{Hg}}^+] &= -k_F [V_{\text{Hg}}^+] [\text{Hg}_l^+] + k_w [W_{\text{Hg}}^x] [\text{Hg}_l^+]; \\ \frac{d}{dt} [W_{\text{Hg}}^x] &= -k_w [W_{\text{Hg}}^x] [\text{Hg}_l^+]; \\ [V_{\text{Hg}}^+] + 2[W_{\text{Hg}}^x] - [\text{Hg}_l^+] &= \delta_0. \end{aligned} \right\} \quad (2)$$

Here square brackets still stand for the concentration of corresponding defects,  $k_F = 4\pi D_l r_F$  and  $k_w = 4\pi D_l r_w$  are constants of the reaction rates between  $\text{Hg}_l^+$  and  $V_{\text{Hg}}^+$  and between  $\text{Hg}_l^+$  and  $W_{\text{Hg}}^x$ , respectively,  $r_F = 4e^2/(k_B T)$  is a  $\text{Hg}_l^+$  capture radius on a Hg vacancy, and  $r_w = a/\sqrt{2}$  is a  $\text{Hg}_l^+$  capture radius on a bivacancy ( $a = 0.648$  nm is the lattice parameter for MCT).

Analysis of the kinetics of defect relaxation showed that at equal concentrations, vacancies relax more quickly than bivacancies, and for the concentrations of vacancy defects at  $t \rightarrow \infty$  the estimations gave  $[W_{\text{Hg}}^x] \approx 0.5 \delta_0$ ;  $[V_{\text{Hg}}^+] \approx (k_w/2k_F)\delta_0 \approx 0.02\delta_0$ . Thus, among the point defects in defect formation zone  $W_{\text{Hg}}^x$  are dominating and

the defect layer contains  $\sim 2 \times 10^{17} \text{ cm}^{-3}$  uncompensated vacancies, which define  $p$ -type conductivity. Therefore, at the border between the defect layer and converted layer there forms a  $p$ - $n$  junction, whose electric field partly hinders penetration of  $\text{Hg}_l^+$  into the bulk of the material.

The average value of  $[\text{Hg}_l^+]_S$  was assessed from the equations of defect relaxation in a defect zone:

$$[\text{Hg}_l^+]_S = \frac{jS}{e} \int_0^\infty [\text{Hg}_l^+](t) dt = \frac{jS}{4\pi e D_l r_w} \ln \frac{2C_{\text{W0}}}{\delta_0}, \quad (3)$$

where  $j/e$  is the frequency of ions hitting the same zone of defect formation, and  $S$  is the effective cross-section of the defect formation zone.

As the defect layer is impermeable for  $\text{Hg}_l^+$ , the sputtered layer (the top 1 nm [41]) cannot act as a source of  $\text{Hg}_l^+$ . Hence, it is the inner part of the defect layer with a thickness of  $\Delta L_0 \sim 1/\sqrt{8\pi r_w C_{\text{W0}}} \sim 0.6$  nm and  $S \sim 2\pi L_d \Delta L_0 \approx 20 \text{ nm}^2$  at  $E \approx 0.5$  keV that acts as the source. According to Eq. (3), at typical IE regimes  $[\text{Hg}_l^+]_S$  is of the order of  $10^{13}\text{--}10^{14} \text{ cm}^{-3}$ , which agrees with estimations from Ref. [43].

### 2.3. Diffusion model of conversion front propagation and its peculiarities in vacancy-doped MCT

To describe the shape of CTC front that was observed in ion-etched MCT with the use of EBIC (with an account for its lateral expansion), the authors of Ref. [24] considered a system of two-dimensional diffusion equations for  $\text{Hg}_l^+$  and  $V_{\text{Hg}}^+$ :

$$\begin{aligned} \frac{\partial c_I}{\partial t} &= D_I \Delta c_I - k_F c_I c_V + S_I \theta(-x) \delta(y); \\ \frac{\partial c_V}{\partial t} &= D_V \Delta c_V - k_F c_I c_V, \end{aligned} \quad (4)$$

where  $c_I(x, y, t)$ ,  $c_V(x, y, t)$  are concentrations of  $\text{Hg}_l^+$  and  $V_{\text{Hg}}^+$ , respectively,  $S_I$  is a function that describes the  $\text{Hg}_l^+$  source, which is located on the surface ( $y = 0$ ,  $x < 0$ ),  $\theta(x)$  is the Heaviside step function,  $\delta(y)$  is the Dirac function,  $\Delta$  is the Laplace operator.

Fitting experimental profiles of CTC front at  $D_I = 2 \times 10^{-6} \text{ cm}^2/\text{s}$ ,  $D_V = 0$ ,  $T_s = 320 \text{ K}$  with the use of these equations allowed for establishing unknown parameters  $S_I$  and  $k_F$ , which secured reproduction of experimentally observed fronts. This seemed to confirm the validity of the diffusion model.

Later [48], to explain the experimental  $d_j(t)$  dependencies reported on in Refs. [35,36] (linear at the first stages transforming into square-root-type at larger  $t$ ), this diffusion model was developed via considering the dependence of  $[\text{Hg}_l^+]_S$  on etching time. Linear dependence at earlier stages was explained by the increase of  $[\text{Hg}_l^+]_S$ , while at later stages this concentration experienced saturation, which resulted in the square-root-type dependence. As an alternative to this explanation, the authors of Ref. [48] also considered a possibility of non-uniform distribution of  $V_{\text{Hg}}^+$ .

The most consistent diffusion model of CTC propagation in ion-etched vacancy-doped MCT was developed in Refs. [40,41]. This model did not require any fitting parameters and described all the experimental observations. Mercury migration in the diffusion layer of MCT subjected to IE does not differ much from diffusion from vapor phase. Thus, for developing the model, the authors considered only two types of defects in the diffusion layer,  $\text{Hg}_l^+$  and  $V_{\text{Hg}}^+$ . As at  $T < 300\text{--}350^\circ\text{C}$  migration of  $V_{\text{Hg}}^+$  can be neglected, one could assume  $D_V = 0$ . Consequently, one should observe a clearly expressed diffusion front, and its propagation is described with effective diffusion coefficient  $D_{\text{Hg}}^* = d_j^2/t$ .

The most important difference between diffusion of  $\text{Hg}_l^+$  under IE and typical diffusion performed from Hg vapor source is related

to the temperature. At 300 K (IE), intrinsic carrier concentration  $n_i$  is much smaller than that at 300 °C (vapor-phase diffusion), so drift of charged defects in the internal electric field of a  $p$ - $n$  junction formed near the surface under IE should be considered.

The equation describing diffusion of  $Hg_I^{+}$  in the converted layer according to [41] was written as:

$$\frac{\partial[Hg_I^{+}]}{\partial t} + \nabla J_{Hg} = -R(\mathbf{r}, t); \quad J_{Hg} \\ = -D_I \left[ \nabla[Hg_I^{+}] + 2 \frac{e}{k_B T_s} [Hg_I^{+}] \nabla \varphi \right], \quad (5)$$

where  $J_{Hg}$  is the density of the diffusion flux of  $Hg$ ;  $R(\mathbf{r}, t)$  is rate for  $Hg_I^{+}$  capture on radiation-induced defects in the damaged layer;  $k_B$  is the Boltzmann constant;  $T_s$  is crystal temperature and  $\varphi$  is electric potential. The elastic energy of  $Hg_I^{+}$  in Eq. (5) was not considered as it was small.

Boundary conditions for Eq. (5) at  $z$  axis were chosen as:

$$[Hg_I^{+}]|_{z=L_d} = [Hg_I^{+}]_S, \quad [Hg_I^{+}]|_{z=d_j} = 0.$$

Conservation law was used [43]:  $J_{Hg}|_{z=d_j} = N_{tr} d(d_j)/dt$ , where  $N_{tr}$  is the concentration of capture centers for  $Hg_I^{+}$  (which are  $V_{Hg}$  in homogeneous vacancy-doped MCT).

Neglecting capture of  $Hg_I^{+}$  in the damaged layer (assuming  $R(r, t)=0$ ) and non-uniformity of the converted layer in relation to  $x$ ,  $N_D$  and  $N_A$ ,  $(4\pi/3)N_I r_0^3 \ll 1$ , where  $N_I$  is the total concentration of the charged centers and  $r_0$  is screening radius, a square-root  $d_j(t)$  dependence was obtained [41]:

$$d_j = l_0 \sqrt{\frac{\Phi}{\Lambda N_{tr}}} \exp\left(-\frac{e\Delta\varphi}{k_B T}\right), \quad (6)$$

where

$$l_0 = \sqrt{\frac{\Lambda S}{2\pi r_w}} \ln\left(\frac{2C_{W0}}{\delta_0}\right); \quad (6a)$$

$\Delta\varphi = \varphi(d_j) - \varphi(L_d)$  is the potential difference between internal ( $z=l$ ) and external ( $z=L_d$ ) boundaries of the converted layer,  $\Lambda = \Phi_0/[V_{Hg}]_0 = 1$  m is a characteristic relation ( $\Phi_0 = 10^{18} \text{ cm}^{-2}$  and  $[V_{Hg}]_0 = 10^{16} \text{ cm}^{-3}$  represent typical values of ion fluence and concentration of  $V_{Hg}$ ).

It is seen that the factor  $l_0$  is barely dependent on the ion energy ( $\sim E_i^{1/6}$ ) and is independent of the  $D_I$ , because  $Hg_I^{+}$  concentration in the diffusion source, according to Eq. (3), is inversely related to  $D_I$ . Hence,  $l_0$  does not depend on the temperature and its dependence on  $x$  is determined by its dependence on  $S$  and, most likely, is weak. Thus, the dependence of  $d_j$  on  $T$  and  $x$  is generally determined by the last (exponential) factor in Eq. (6). Assuming, according to the estimations obtained above, that  $S = 2 \times 10^{-13} \text{ cm}^2$ ,  $C_{W0} = 2 \times 10^{20} \text{ cm}^{-3}$ , and  $\delta_0 = 10^{19} \text{ cm}^{-3}$ ,  $l_0$  was assessed as  $\sim 160 \mu\text{m}$ .

The distribution of the potential  $\varphi$  in the structure could be found on the basis of the one-dimensional Poisson equation in the continuous form ( $N_\Sigma = N_D - N_A$ ):

$$\frac{d^2\varphi}{dz^2} = \frac{e}{\epsilon_1 \epsilon_0} (n - p - N_\Sigma), \quad (7)$$

As the thickness of the defect layer  $L_d$  is of the order of the screening length, one could not solve Eq. (7) analytically. Thus,  $\varphi$  was calculated by solving the equation numerically. According to the above listed estimations for the vacancy concentration in the defect layer, it was assumed that  $N = -4 \times 10^{17} \text{ cm}^{-3}$  at  $0 < z < L_d$ . In the conversion layer ( $z > L_d$ ) donor concentration was taken as  $N_D = 1 \times 10^{15} \text{ cm}^{-3}$ , which is a typical value in the experi-

ment. Since the  $Hg_I^{+}$  concentration in the conversion layer is small ( $\sim 10^{13} \text{--} 10^{14} \text{ cm}^{-3}$  [43]), these defects were not considered.

Calculations showed (Fig. 4) that  $\Delta\varphi = \varphi(\infty) - \varphi(L_d)$  increases with  $x$  increasing. Thus, the electric field at the interface between the defect layer and the converted layer hindered the diffusion of positively charged  $Hg_I^{+}$  atoms into the crystal and, therefore, CTC depth decreased with  $x$  increasing and/or temperature decreasing.

An alternative explanation of the observed  $d_j(t)$  dependencies at IE (Fig. 1) for a time-independent  $[Hg_I^{+}]_S$  [48] and without introducing surface  $p$ - $n$  junction was proposed in Ref. [14]. It was assumed that the conversion process was a quasi-stationary one, so steady-state equations were used. Because  $[Hg_I^{+}]$  is much smaller than the initial vacancy (acceptor) concentration, the active conversion region was considered to be narrow, so a sharp boundary was introduced at  $x_j$  between the converted and unconverted regions of MCT. The conversion rate  $dx_j/dt$  was then controlled by the diffusion rate of  $Hg_I^{+}$  to the conversion boundary at  $x_j$  and by the capture rate of the interstitials by cation vacancies at  $x_j$ . These rates acted in tandem so that the overall conversion rate was determined by the slower of the two. Two cases were considered: (1) intrinsic MCT, where at room temperature the initial acceptor concentration is smaller than intrinsic concentration (at 300 K  $\sim 3 \times 10^{16} \text{ cm}^{-3}$  and  $\sim 4 \times 10^{15} \text{ cm}^{-3}$  for  $x=0.20$  and 0.30, respectively), so under IE there would be no depletion layer due to a  $p$ - $n$  junction at  $x_j$ ; and (2) extrinsic MCT, when the opposite was the case. Effect of sample heating was neglected.

For intrinsic MCT equation for  $Hg_I^{+}$  flux  $J$  across the converted layer at steady-state conditions was written as  $J = D_I(C_0 - C_j)/x_j$ , where  $C_0$  and  $C_j$  were  $Hg_I^{+}$  concentrations at  $x=0$  and  $x=x_j$ , respectively.  $Hg_I^{+}$  atoms arriving at the unconverted boundary  $x_j$  were captured by cation vacancies at a rate  $k_j C_j N_A$ , where  $k_j$  is the capture coefficient for  $Hg_I^{+}$  by the vacancies with initial concentration  $N_A$  that was assumed to be uniform. From equation for  $J$  in Ref. [14] the following relation was obtained:

$$k_j N_A x_j^2 + 2D_I x_j = 2k_j D_I C_0 t. \quad (8)$$

Eq. (8) had two limiting forms:  $x_j \sim t$  when  $2D_I \gg k_j N_A x_j$ , and  $x_j^2 \sim t$  when  $2D_I \ll k_j N_A x_j$ . This meant that in the initial period of CTC the capture rate of  $Hg_I^{+}$  at  $x_j$  was the controlling factor. As  $x_j$  increases, the diffusion rate decreased and became the controlling factor.

Within the frames of the ‘intrinsic MCT’ model the authors of Ref. [14] analyzed experimental data on  $d_j(t)$   $x_j(t)$  presented in Refs. [11,24,25,32] and shown in Fig. 1. For example, the data from Refs. [11] and [32] fitted to Eq. (8) yielded  $3.26 \times 10^6 x_j^2 + 1.15 \times 10^5 = t$  and  $2.00 \times 10^7 x_j^2 + 1.65 \times 10^5 = t$ , respectively, where  $x_j$  was in centimeters and  $t$  in seconds. The analysis yielded  $k_j C_0 = 8.7 \times 10^{-6} \text{ cm s}^{-1}$ ,  $D_I C_0 = 1.5 \times 10^9 \text{ cm s}^{-1}$  and  $C_0 = 2 \times 10^{14} \text{ cm}^{-3}$  for the data from Ref. [11], and  $k_j C_0 = 6.2 \times 10^{-6} \text{ cm s}^{-1}$ , and  $D_I C_0 = 2.8 \times 10^8 \text{ cm s}^{-1}$  for the data from Ref. [32].

For the data from Ref. [24] with IE with neutral Ar beam the  $d_j(t)$  dependencies were close to parabolic ones with  $C_0$  between  $9.5 \times 10^{13} \text{ cm}^{-3}$  and  $1.3 \times 10^{14} \text{ cm}^{-3}$ , which agreed well with the data from Ref. [11]. But for the data from Ref. [25] of the same authors with Ar RF plasma etching, the  $d_j(t)$  dependencies were close to parabolic ones with  $C_0 = 1.2 \times 10^{15} \text{ cm}^{-3}$ .

For extrinsic MCT the pattern becomes more complicated as one needs to consider formation of a space charge layer at  $x_j$ . According to Ref. [14], between  $x=0$  and some  $x_s$ , there is a narrow extrinsic  $n$ -type layer, possibly due to Te antisite defects (of unclear origin), followed by the intrinsic type-converted region between  $x_s$  and  $x_n$  that at 77 K is  $n$ -type due to ‘high’  $N_D$ . The presence of the  $n$ -type layer between  $x=0$  and  $x_s$  ensures that the depletion layer does not extend to  $x=0$ . The rest of the converted region should lie between  $x_n$  and  $x_j$  and define the positive space-charge side of the  $p$ - $n$  junc-

tion due to the ionized residual donors. The negative space-charge region of the junction lies between  $x_j$  and  $x_p$  with ionized acceptor concentration  $N_A$ . The depletion layer of the  $p$ - $n$  junction therefore lies between  $x_n$  and  $x_p$ . Steady-state conditions were assumed so  $J$  was constant between  $x=0$  and  $x_j$ . In the region  $0 < x < x_n$  the  $Hg_i^{..}$  flux arises from diffusion down the concentration gradient, so  $J = D_I(C_0 - C_n)/x_n$ , where  $C_n$  is the  $Hg_i^{..}$  concentration at  $x_n$ . In the depletion layer  $x_n < x < x_j$  the flux has two components, one being due to the concentration gradient and the other being due to the electric field  $E(x)$ . The flux component due to the electric field is given by  $\mu E(x)C$  where  $\mu$  is the drift mobility of the  $Hg_i^{..}$  interstitial. Therefore:

$$J = D_I dC/dx + \mu E(x)C. \quad (9)$$

In Ref. [14] it was assumed that  $p$ - $n$  junction was abrupt, so  $E(x) = eN_D(x - x_n)/\epsilon\epsilon_0$ , where  $\epsilon$  is the static dielectric constant of MCT. The integration of Eq. (9) gives  $C$  versus  $x$ , and  $x_j, x_n$  versus  $t$ :

$$x_n^2 + 2[(D_I/k_j N_A) \exp(-Bl^2/2) + I(l)]x_n = 2D_I C_0 t/N_A, \quad (10)$$

where  $B = 2e^2 N_D/\epsilon\epsilon_0 kT$ ;  $I(l) = (1/\beta) \int_0^\beta \exp(-z^2) dz$ ;  $l^2 = (2\epsilon\epsilon_0 kT/e^2)[N_A/(N_D(N_A + N_D))] \ln(N_A/n_i)$  and whose magnitudes will vary with  $N_D$  and  $N_A$ . Eq. (10) is applicable only when the depletion layer on the  $n$ -side of the  $p$ - $n$  junction is determined by  $N_D$  and the depletion layer does not penetrate into the extrinsic  $n$ -type surface region i.e.  $x_n \geq x_s$  and it is assumed that  $x_s$  is negligible relative to  $l$ .

As there were no reliable experimental data on  $d_j(t)$  for MCT with  $x \sim 0.3$  (extrinsic case), it appeared to be not possible to apply the proposed model to such material. Nevertheless, the analysis performed in Ref. [14] showed that in this case the conversion rate showed the behavior similar to that in the intrinsic case in that  $x_j^2 \sim t$  and  $x_j \sim t$  for large and small  $x_j$ , respectively.

In Ref. [14] the authors also considered a possibility of the presence, along with  $V_{Hg}$ , of some additional capture centers with concentration  $N_{tr}$  with trapping rate  $k_t C_j N_{tr}$  ( $k_t$  is the capture coefficient for Hg interstitials by the empty trap) and their effect on  $d_j(t)$  under IE. As will be shown below, such centers may be in fact represented by residual I- and V-group acceptors, which under IE form donor centers with  $Hg_i^{..}$ . The authors of Ref. [14] considered both the intrinsic case and the extrinsic situation, and it was shown that the quadratic relation between  $x_j$  and  $t$  was still valid: trapping caused equality between the parabolic and linear terms at smaller  $x_j$ . For example, it was shown that in the intrinsic case the ratio of the coefficients gave  $D_j/k_j(1+\alpha)$  compared to  $D_j/k_j$  in the absence of trapping (where  $\alpha = k_t N_{tr}/k_j N_A$ ). Assuming that trapping affected the data from Refs. [11,25,32], the authors decided that trapping could explain the observed variations in  $D_j/k_j(1+\alpha)$  due to differences in  $\alpha$ .

#### 2.4. The dependence of the conversion depth on MCT composition and temperature

The dependence of CTC depth on MCT composition  $x$  in vacancy-doped material was studied in Refs. [33,41]. It was established that the depth decreases with  $x$  increasing in the composition range  $x = 0.16$ – $0.39$ , all other conditions being the same. The results are presented in Fig. 3.

The reduced conversion depth  $d_r$  was calculated as experimental  $d_j$  reduced to  $[V_{Hg}]_0 = 10^{16} \text{ cm}^{-3}$  and ion fluence  $\Phi_0 = 10^{18} \text{ cm}^{-2}$  using  $d_r = d_j \sqrt{A \cdot [V_{Hg}]}$  relation. It should be noted that IE used in Ref. [33] was performed with neutralized ions without sample cooling. In this case, sample temperature during IE can reach 50–70 °C. In experiments described in Ref. [41], sample holder used for IE in DC  $Ar^+$  plasma was cooled with water, so sample temperature was close to 300 K.

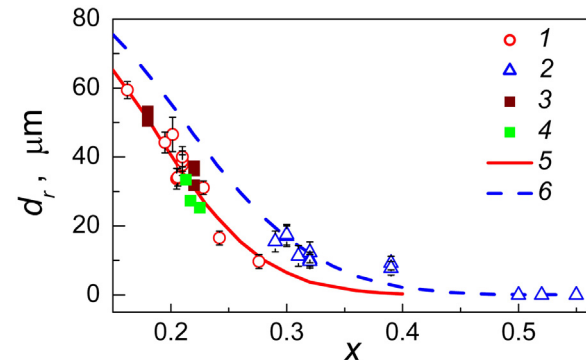


**Fig. 3.** The dependence of the reduced conversion depth  $d_r$  on the composition in  $p$ -MCT. Points show experimental data for: vacancy-doped MCT, 1 [41] and 2 [33]; As- or Sb-doped MCT, 3 [65,66]; Cu-, Ag- or Au-doped MCT, 4 [77]. Lines show results of calculations performed in Ref. [41] for temperatures 293 K (5) and 340 K (6).

It is seen in Fig. 3 that the calculated values of  $d_r$  agree well with those experimentally observed, if factor  $l_0$  in Eq. (6a) is assumed to be  $l_0 = 123 \mu\text{m}$ . This  $l_0$  value obtained by fitting was quite close to  $l_0 \approx 160 \mu\text{m}$  derived theoretically. This strongly supports the validity of the proposed diffusion mechanism of  $Hg_i^{..}$  source formation and CTC front propagation. Therefore, it is the dependence of  $\Delta\varphi$  on  $x$  that defines  $d_j(x)$  dependence in compositionally uniform MCT observed in the experiment. The  $d_j$  value monotonically decreases with  $x$  increasing in both sets of experiments. The dependencies do not coincide, which is mostly likely caused by the different temperatures of the samples during IE. Thus, it can be concluded that  $d_j$  in  $p$ -MCT increases with temperature increasing, which agrees with the results presented in Ref. [27]. Calculations of  $d_j(T)$  dependence performed within the frames of diffusion model in Ref. [41] for the data of Ref. [27] gave a good agreement between the experiment and the model. Thus, CTC in vacancy-doped  $p$ -MCT under IE is conditioned by diffusion of  $Hg_i^{..}$  atoms from surface source with extremely high non-equilibrium concentration, and their annihilation with intrinsic acceptors  $V_{Hg}$  that determined  $p$ -type conductivity of initial sample. In the converted  $n$ -layer satisfied is the mass action law:  $[V_{Hg}] \cdot [Hg_i^{..}] = K_F$ . At 300 K  $K_F \sim 10^7 \text{ cm}^{-6}$  and  $[Hg_i^{..}] \sim 10^{14} \text{ cm}^{-3}$ , so  $[V_{Hg}] \rightarrow 0$ . This implies that in the main part of the converted  $n$ -layer the vacancies are practically absent, in contrast to CTC in vacancy-doped  $p$ -MCT thermally annealed in mercury vapors.

#### 2.5. Effect of wide-bandgap protective layers on propagation of conversion front

The development of MCT epitaxial technology (MBE and MOCVD) allowed for fabricating device structures with  $Hg_{1-y}Cd_yTe$  ( $y \gg x_a$ ) WBPLs deposited *in situ*. Naturally, the effect of WBPL on CTC under IE had to be studied. In reality, first experiments on IE of MCT with WBPL were performed in Refs. [35,36], however, the effect of WBPL on the conversion front propagation was not considered.

Experimental proofs of the effect of WBPL on CTC depth under IE were obtained in Ref. [37], where heteroepitaxial MBE-grown (GaAs substrate) MCT structures ( $x_a = 0.22$ ) with WBPL were studied. The thickness of the active layer varied from 6 up to  $8.5 \mu\text{m}$ . The active layer was sandwiched between graded-gap WBPLs with composition  $y$  gradually increasing, throughout a  $1.5 \mu\text{m}$ -thick layer, up to  $y = 0.4$ . The structures were subjected to IE with  $Ar^+$  ions with  $E = 500 \text{ eV}$ ,  $j = 0.25$ – $0.3 \text{ mA/cm}^2$  and  $t = 300$ – $720 \text{ s}$  (with water cooling of the sample holder down to 21 °C). The CTC depth in the structures with WBPL intact was less than  $5 \mu\text{m}$  and depended on  $[V_{Hg}]$  ( $10^{16}$ – $10^{17} \text{ cm}^{-3}$ ). This depth was substantially lower than

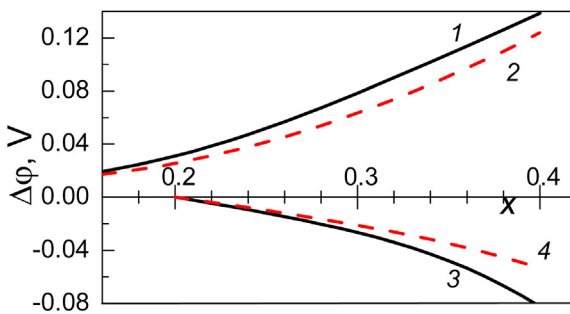


**Fig. 4.** The calculated dependence of the potential difference of the defect layer field  $\varphi_1$  (curves 1, 2) and of the potential of a graded-gap WBPL  $\varphi_2$  (3, 4) on the composition of the WBPL  $y$  in MCT structure with  $x_a = 0.2$  at  $T = 293\text{ K}$  (1, 3) and  $345\text{ K}$  (2, 4) (after [41]).

the value that could be expected in MCT samples with uniform composition corresponding to  $x_a$ . After WBPLs were removed, IE lead to CTC throughout the whole thickness of the active layer. Therefore, it was unambiguously established that the presence of WBPL considerably decreases CTC depth. Also, in Ref. [34] it was shown that in a CdTe/*p*-Hg<sub>1-x</sub>Cd<sub>x</sub>Te structure ( $x_a = 0.23$ ) grown with MOCVD with the thickness of CdTe WBPL  $\sim 1\text{ }\mu\text{m}$ , there was no CTC after IE at all.

The nature of the effect of WBPL on the CTC depth was studied in Ref. [41]. In epitaxial structures with WBPL density of states in the conduction band  $N_C$  and energies of the conduction  $E_C$  and valence  $E_V$  bands depend on coordinate  $z$  via their dependence on composition  $y$ . This has a drastic effect on the distribution of the potential of the internal electric field, which affects CTC depth. In reality, the thickness of the protective layer  $L_y \sim 1\text{ }\mu\text{m}$  is usually large as compared to the screening length  $r_0$  in the layer, and  $y$  does not change noticeably within the distance of a few  $r_0$ , as counted from the inner boundary of the defect layer  $z = L_d$  (Fig. 2). Having this in mind, the potential  $\varphi(z)$  can be presented as a sum of the two items:  $\varphi(z) = \varphi_1(z) + \varphi_2(z)$ , where  $\varphi_1(z)$  is a potential of a *p-n* junction equal to that in compositionally uniform MCT with  $x = x(L_d)$ ;  $\varphi_2(z)$  is an equilibrium potential of an *n*-MCT structure with given distribution of impurity  $N(z)$  and composition  $y(z)$ .

In the approximation of a microscopically uniform conversion layer the potential  $\varphi_2(z)$  can be calculated by solving electro-neutrality equation:

$$n - p - N = 0, \quad (11)$$

where for  $n$ ,  $p$  and  $N_C$  it is assumed that  $E_C$  and  $E_V$  are functions of  $y$ .

The calculations showed (Fig. 4) that for MCT structures with WBPL  $\varphi_2(l) < \varphi_2(L_d)$ , i.e., the electric field of the graded-gap structure, in contrast to the field  $\varphi_1(z)$  of *p-n* junction, favors Hg<sub>*y*</sub> diffusion into the converted layer under IE. Still, the total potential difference  $\Delta\varphi$  remains positive, which means that the total electric field of the structure yet hinders the diffusion. The explicit dependence of  $d_j$  on the fluence  $\Phi$  and potential  $\varphi$  was calculated by the authors of Ref. [41] under conditions when the potential fluctuations were small,  $R = 0$ ,  $l > L_y \gg r_0$  and  $y$  in WBPL did not change at the order of  $r_0$  as counted from the plane  $z = L_d$  (Fig. 2):

$$d_j = \sqrt{l_0^2 \frac{\Phi - \Phi_L}{\Lambda N_{tr}} \exp\left[-\frac{2e\Delta\varphi}{k_B T}\right] + L_u^2} - L_u + L_y, \quad (12)$$

where  $\Delta\varphi = \varphi(l) - \varphi(L_d)$ ;  $\Delta\varphi_2 = \varphi_2(l) - \varphi_2(L_d)$ ;  $\Phi_L = jt_L/e$  (point  $t_L$  is defined by the condition  $d_j(t) = L_y$ ).

The conversion depth  $d_j$  and constants  $L_u$  and  $\Phi_L$  in Eq. (12) depend on the actual composition distribution law in the structure.

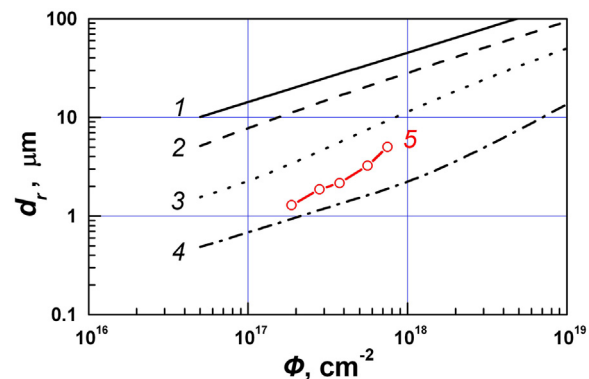


**Fig. 5.** Calculated dependences of the reduced conversion depth on ion fluence for an ion-etched MCT structure with WBPL with  $x_0 = 0.20$  (curve 1), 0.25 (2), 0.30 (3) and 0.35 (4). Curve 5 shows experimental dependence for the structure with  $x_0 = 0.22$  and  $x_y = 0.48$  (after [49]).

In particular, for a step-like distribution ( $y = y_1$  at  $z < L_y$  and  $y = y_2$  at  $z > L_y$ ):

$$\Phi_L = \frac{l_y^2}{l_0^2} \Lambda N_{tr} \exp\left[-\frac{2e\Delta\varphi_1}{k_B T}\right]; \quad L_u = L_y \cdot \exp\left(-\frac{2e\Delta\varphi_2}{k_B T}\right). \quad (13)$$

Due to the effect of the drift of charged intrinsic defects in the electric field of the graded-gap WBPL, the dependence of  $d_j$  on  $\Phi$  at  $L_y < d_j \ll L_u$  (i.e., for the protective layer with high composition) becomes almost linear and is inversely related to  $N_{tr}$ :

$$d_j \approx L_y + \frac{(\Phi - \Phi_L)l_0^2}{2\Lambda N_{tr}L_u} \cdot \exp\left(-\frac{e\Delta\varphi}{k_B T}\right). \quad (14)$$

It was this type of  $d_j(\Phi)$  behavior that was reported in Refs. [35,36], where CTC depth under IE was studied as a function of ion dose ( $D = e\Phi$ ) for MBE-grown structures with WBPL. It was shown [41] that the calculated dependence of  $d_j$  on  $D$  fits well the experimental data. Thus, it is the electric field of the graded-gap structure that accounts for the linear dependence of the conversion depth on IE time under small ion doses. This explanation does not require any speculative assumptions, like time-dependent saturation of the mercury source or gradient of  $[V_{Hg}]$ , as was suggested in Ref. [48].

The effect of graded-gap WBPL on CTC under IE in MBE-grown *p*-MCT structures was studied in Ref. [49]. The structures had similar  $x_a \approx 0.22$  and the thickness of the graded-gap layer  $L_y \sim 1.7\text{ }\mu\text{m}$ , but different composition on the surface  $x_y$ : 0.22 (without WBPL), 0.35, 0.48 or 0.56.

Fig. 5 shows the calculated dependences of  $d_j$  on  $\Phi$  for ion-etched MCT structure with  $x_a = 0.20$  and three 1.7 μm-thick WBPLs with different  $x_y$ , calculated according to the above model. It can be seen that  $d_j$  decreases with  $x_y$  increasing. Fig. 5 also shows experimental fluence dependence of the CTC depth (reduced to  $[V_{Hg}] = 1 \times 10^{16}\text{ cm}^{-3}$ ) for structure with  $x_y = 0.48$ .

For sample without WBPL, CTC took place throughout the whole thickness of the structure (10.8 μm) for all the fluences used. This result agrees with the calculated values of  $d_j > 10\text{ }\mu\text{m}$  (Fig. 5, curve 1). For sample with  $x_y = 0.35$  conversion also took place throughout the whole thickness of the structure (10.1 μm) for all the ion fluences; thus, experimentally conversion depth was larger than that predicted by calculations (Fig. 5, curve 4). We should consider, however, that IE actually sputters the surface layer of the material: in this sample IE at  $j = 0.1\text{ mA/cm}^2$  and  $t = 20\text{ min}$  etched off  $\sim 0.3\text{ }\mu\text{m}$  of MCT. Considering composition grading, at such etching for the structure with  $x_y = 0.35$  at the end of IE  $x_y$  approached 0.28, which should yield conversion deeper than the thickness of this structure. This agreed with the results of the calculations performed for  $x_y = 0.25$  (curve 2). Similar analysis applies for structure with

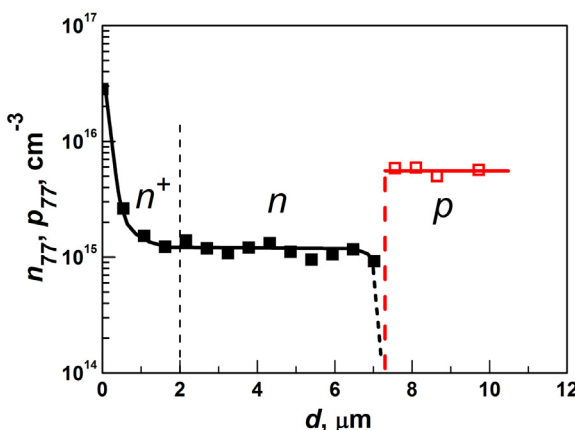


**Fig. 6.** Carrier concentration profile in ion-etched MCT with WBPL. Filled symbols correspond to electrons, empty symbols relate to holes (after [49]).

$x_y = 0.48$  (curve 5). Considering the etched-off layer and the precision of determination of CTC with step-by-step chemical etching, the experimental dependence agreed with calculations performed for MCT structure with  $x_y = 0.30$  to  $x_y = 0.35$  (curves 3 and 4).

Therefore, the experimental data confirmed the validity of the model, which predicted the effect of the graded-gap WBPL on the CTC depth under IE via the influence of the internal electric fields of the  $p$ - $n$  junction in the defect layer and graded-gap layer, which defined diffusion of  $Hg_i$  into the crystal.

## 2.6. Electrical properties of ion-etched MCT

Electrical properties of ion-etched MCT have been studied for both uniform samples and those with WBPL [16,20,22,24,25,29–32,37,41,49–52]. As was shown by many authors, the converted/modified  $n$ -layer is not uniform. For example, Fig. 6 shows carrier concentration profile in ion-etched MBE-grown  $p$ -MCT sample with WBPL ( $x_y = 0.48$ ) with hole concentration at 77 K  $p_{77} \approx 6 \times 10^{15} \text{ cm}^{-3}$  after IE ( $E = 500 \text{ eV}$ ,  $j = 0.1 \text{ mA/cm}^2$ ,  $t = 5 \text{ min}$ ) after Ref. [49]. The profile was recorded ~1.5 years after IE.

A thin surface layer (~1–3 μm) has high electron concentration ( $n_{77} \approx 10^{17}$ – $10^{18} \text{ cm}^{-3}$ ) and low mobility ( $\mu_{n77} \sim 10^4 \text{ cm}^2/(\text{Vs})$ ). In this layer, concentration decreases toward its depth while mobility increases. We shall designate this layer as ' $n^+$ -layer' and also shall refer to it as to the 'damaged' layer. This layer is followed by a  $n$ -layer with thickness that depends on  $N_A$ ,  $x$  and IE parameters ( $j$ ,  $t$ ,  $T_s$ ). The layer has constant values of  $n_{77}$  and  $\mu_{n77}$  throughout its thickness. We shall refer to this layer as to ' $n$ -layer' and call it the 'bulk' converted/modification layer. Values of hole concentration  $p_{77}$  and mobility  $\mu_{p77}$  in unconverted part of MCT are the same as those in the sample before IE. Thus, IE of  $p$ -type MCT generally results in the formation of  $n^+$ - $n$ - $p$  structure. This conclusion was made on the basis of the results obtained with the use of differential Hall-effect measurements with step-by-step chemical etching. In Ref. [29], the non-uniform electron concentration distribution in IE-converted MCT was established with the use of capacitance-voltage measurements. Similar type of distribution was pointed out to also by the results of the study of lifetime of non-equilibrium carriers  $\tau$  [16,20,22,31]. In each case it was established that in the damaged  $n^+$ -layer  $\tau$  was much lower than that in the 'bulk'  $n$ -layer.

It is believed that the appearance of  $n^+$ -layer is caused by radiation defects formed by energetic ions. For example, in Ref. [29] it was suggested that ions interacting with MCT surface result in high density of extended defects, such as dislocation loops. Formation of  $n^+$ -layer was detected in experiments on reactive IE in RF

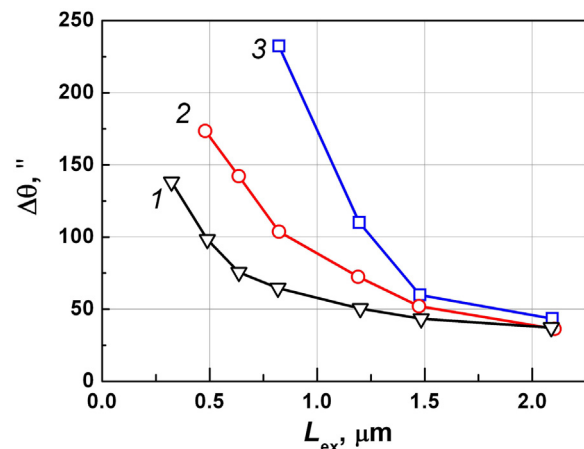


**Fig. 7.** The dependence of the FWHM of rocking curves  $\Delta\theta$  at (511)-reflex on the depth of X-ray penetration in MCT subjected to IE in RF plasma with bias: curve 1, 0.6 kV; 2, 1.2 kV; 3, 2.4 kV (after [57]).

$H_2/CH_4$  plasma of LPE-grown  $p$ -MCT ( $x = 0.3$ ) with the use of the measurements of laser-beam induced current (LBIC) with step-by-step chemical etching [53]. The existence of the damaged  $n^+$ -layer also followed from the analysis of the field dependencies of the Hall coefficient and conductivity performed with various modifications of the mobility spectra analysis (MSA) [49–54]. It was shown in Refs. [53,54] that  $n_{77}$  and  $\mu_{n77}$  in the damaged layer did not depend on the temperature in the range 20–300 K.

Data on structural perfection of the  $n^+$ -layer are very limited. In Ref. [55], defect structure of the cleft edge of  $Hg_{0.7}Cd_{0.3}Te/CdTe$  heterostructures subjected to IE ( $E = 4 \text{ keV}, j = 3.5 \text{ mA/cm}^2$ ) was studied with transmission electron microscopy. It appeared that concentration of defects (dislocations and dislocation loops) in MCT was 2–3 orders of magnitude lower than that in CdTe. The authors of Ref. [55] related this phenomenon to high rate of defect annihilation in MCT. Radiation damage in a form of chaotic dislocations and dislocation loops with ~40 nm in diameter was also detected with transmission electron microscopy in ion-etched MCT in Ref. [56]. Dislocations were located at the depth of 50 nm from the surface and relaxed in 4 weeks at 300 K.

The distribution of structural defects in the damaged  $n^+$ -layer was studied in Ref. [57] with the use of X-ray diffraction analysis performed on graded-gap (111)  $n$ -MCT ( $x = 0.2$ ) 50 μm-thick films (Fig. 7). The films were subjected to IE in RF Hg plasma at biases 0.6, 1.2 and 2.4 kV with etching time 15, 5 and 1 min, respectively. Under these conditions, in each case IE sputtered off a 0.5 μm-thick surface layer. It is seen in Fig. 7 that full-width at half-maximum (FWHM) of reflex decreased from the surface into the bulk of the samples, which was indicative of the decrease of the density of structural defects formed with IE. Increasing the bias (Hg ion energy) caused the increase in the depth of propagation of structural damage, and the degree of structural disorder was decreasing with depth  $z$  as  $\exp(z/\lambda)$  with  $\lambda \approx 0.5 \text{ μm}$ . This dependence corresponded to that of  $n_{77}$  in the  $n^+$ -layer with a similar coefficient  $\lambda$ .

A process responsible for  $n$ -type conductivity of the damaged  $n^+$ -layer was proposed in Ref. [41,58]. It was suggested that donor defects in the damaged  $n^+$ -layer were formed when  $Hg_i$  was captured by the cores of dislocations. Details of the mechanism are given in Section 2.8.

The bulk of converted/modification  $n$ -layer typically has low  $n_{77}$ , which, according to various authors, lies in the range  $\sim 10^{14}$ – $5 \times 10^{15} \text{ cm}^{-3}$  [11,15,17,20,22,24,29,31,32,36,49–54,59]. Most authors agree that this concentration is defined by residual donors and thus can vary from sample to sample. Residual donors

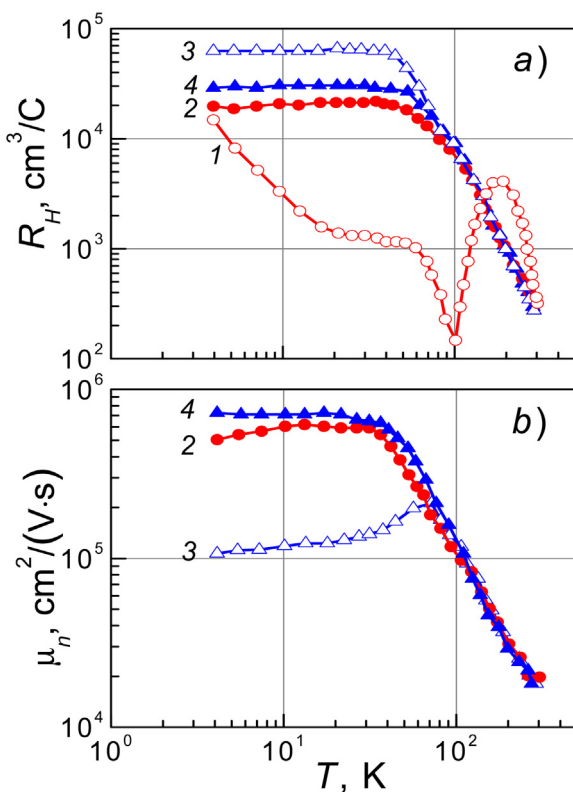


**Fig. 8.** Temperature dependences of  $R_H$  (a) and electron mobility (b) in LPE-grown  $p$ - (curves 1 and 2) and  $n$ -type MCT (3 and 4) [32]: 1 and 3, before IE; 2 and 4, after IE. Mobility for initial  $p$ -type sample is not shown. 1,  $R_H$  with sign inversion; 2–4,  $R_H < 0$ .

may be represented by background donor doping typical of specific growth technology and, perhaps, by intrinsic donor defects such as antisite tellurium [32,33,37], typical of MBE-grown MCT, on this see below.

Let us make an important notice on the values of  $n_{77}$  and  $\mu_{n77}$  in the bulk  $n$ -layer formed after IE. In all the papers cited above (except for those by the authors of this review [49–52,59]) there was no consideration for the effect of relaxation of electrical parameters of MCT (decrease in conductivity and  $n_{77}$ ) after IE, which was first reported on back in 2001 [28]. In reality,  $n_{77}$  and  $\mu_{n77}$  as measured after IE strongly depend on time which has passed from the moment of IE up to the moment of the measurement. True values of  $n_{77}$  and  $\mu_{n77}$  in the converted/modified  $n$ -layer can be determined only after the relaxation of the parameters, which typically takes  $10^4$ – $10^5$  min; this matter will be discussed in detail below.

The bulk  $n$ -layer usually has high  $\mu_{n77}$  ( $100,000$ – $250,000 \text{ cm}^2/(\text{Vs})$ ) for MCT with  $x=0.20$ – $0.23$ , which is typical of high-quality MCT with low electrical compensation [11,20,22,24,31,32,36,49,52–54]. Temperature dependences of carrier concentration and mobility in the bulk  $n$ -layer (Fig. 8) also correspond to classic behavior of these parameters in  $n$ -MCT with low compensation [24,31]. In the temperature range 77–4.2 K, the Hall coefficient  $R_H$  and electron mobility do not depend on  $T$ , while with temperature increasing they both decrease. The slope of the  $R_H(T)$  dependence coincides with  $E_g/2$ , i.e., reflects activation of intrinsic conductivity, while  $\mu_n(T)$  behavior is typical of phonon scattering.

The bulk  $n$ -layer formed in MCT with initial  $p$ -type has relatively large values of  $\tau$ , 1–3  $\mu\text{s}$  at 77 K for MCT with  $x\sim 0.2$  [20,22,31,32]. These  $\tau$  values speak of low degree of electrical compensation, too.

Effect of IE on the properties of  $n$ -MCT was studied in Refs. [23,29,31,32,37,50–52]. This effect is expressed in lowering the

degree of electrical compensation due to annihilation of residual  $V_{\text{Hg}}$  and transformation of background I- and V-group acceptors into donors. This is confirmed by the changes in concentration, mobility and lifetime of electrons in the modified layer. For samples with initial low compensation, IE resulted in increasing both  $n_{77}$  and  $\mu_{n77}$  [29,32,50–52]. For strongly compensated samples that showed a typical maximum at  $T\leq 77$  K on  $\mu_n(T)$  dependencies, after IE the behavior of  $\mu(T)$  became typical of high-quality MCT with low degree of compensation (Fig. 8b, curves 3 and 4).

### 2.7. Conductivity type conversion in MCT doped with I- and V-group acceptors

The authors of Refs. [53,60–62] were the first to establish that CTC under IE can be observed not only in vacancy-doped MCT, but also in  $p$ -type material obtained with doping with As or Au. On the one hand, these elements are regarded as basic acceptor dopants for fabricating extrinsic  $p$ -MCT for photodiode structures [63]. On the other hand, acceptors of I group (Cu, Ag, Au) and V group (As, Sb) are most frequent background impurities in MCT, and they often cause high degree of compensation in  $n$ -type material. For example, it was the arsenic impurity that supposedly caused relaxation of parameters of the converted  $n$ -type layer after IE in vacancy-doped MCT in Ref. [28].

#### 2.7.1. Conductivity type conversion in MCT doped with As and Sb

CTC in  $p$ -MCT doped with arsenic was observed by the authors of Refs. [60–62] when they studied the effect of reactive IE in RF  $\text{CH}_4/\text{H}_2$  plasma on LPE-grown  $p$ -MCT films with  $x\approx 0.3$ . Doping was performed during the growth. After the growth, samples were annealed at low temperature in mercury vapors, so  $V_{\text{Hg}}$  were eliminated and  $p$ -type conductivity of the films ( $p_{77}\approx 2\times 10^{16} \text{ cm}^{-3}$ ) was defined by arsenic atoms in anion sublattice. The fact of CTC under IE was established with the use of LBIC, and it was found that CTC proceeded throughout the whole thickness of the films ( $\sim 7 \mu\text{m}$ ). Electrical parameters of the films were not studied; however, analysis of the shape of the LBIC signal allowed the authors of Refs. [60–62] to conclude that  $n_{77}$  in the converted films was close to  $p_{77}$  (and thus, arsenic concentration  $N_{\text{As}}$ ) measured before IE. It was also shown in Ref. [62] that annealing of the converted films in mercury vapors at 200 °C for 17 h resulted in CTC back to  $p$ -type with parameters corresponding to those of initial films. The mechanism of CTC under IE was not considered.

The authors of Refs. [64–66] studied CTC under IE in DC Ar plasma ( $E=500$  eV) in  $p$ -MCT doped with either As or Sb, and this allowed them to establish more general pattern of conversion. Graded-gap epitaxial  $p$ -MCT films autodoped with As ( $x=0.22$ ;  $p_{77}=3\times 10^{16} \text{ cm}^{-3}$ ) or Sb ( $x=0.18$ ;  $p_{77}=1.8\times 10^{16} \text{ cm}^{-3}$ ) from CdTe substrates were grown with isothermal vapor-phase epitaxy (ISOVPE). After the growth films were *in situ* annealed at low temperature in mercury vapors to minimize  $[V_{\text{Hg}}]$ . As was shown in Ref. [67], for understanding CTC processes in MCT doped with As or Sb, it was necessary to study the relaxation of electrical parameters in the converted material. The existence of such relaxation even at 300 K in MCT doped with As was experimentally proven in Ref. [68], yet was not considered in previous works [60–62,64–66], which caused some problems with interpretation of experimental results, e.g., in Refs. [65,66].

The results of the studies of relaxation at 300 K are presented in Fig. 9 [67,68]. The inset shows that after IE integral values of  $\sigma$  and  $R_H$  experienced strong relaxation. Negative  $R_H$  values for all magnetic field values  $B$  used spoke of the formation of  $n$ -type layers, i.e., of the appearance of some donor defects. The shape of  $R_H(B)$  dependencies was indicative of the existence of electrons with high and low mobility, i.e., of the formation of a typical  $n^+ - n - p$  structure with damaged  $n^+$ -layer and bulk  $n$ -layer, which was confirmed by

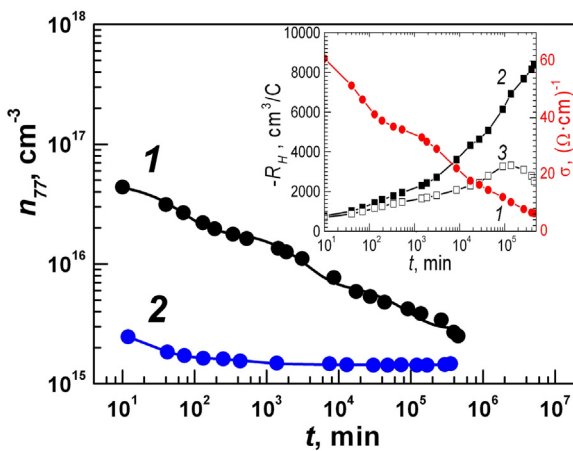


**Fig. 9.** Dependence of  $n_{77}$  on the storage time at 293 K for ion-etched MCT samples doped with As (curve 1) and Sb (2). Points represent experimental data while solid lines show the results of calculations. Inset shows time dependencies of integral conductivity (curve 1) and  $R_H$  (2,  $B=0.05$ ; 3,  $B=1.0$  T,  $R_H < 0$ , 77 K) after IE for the sample doped with As [67].

the MSA data. Obviously, the relaxation should be considered when establishing carrier concentration profiles with chemical etching [67].

The CTC depth in these samples corresponded to that in vacancy-doped MCT with similar  $x$  under similar IE conditions (Fig. 3) [67]. Relaxation of  $n_{77}$  for both types of samples was exponential with three (for arsenic-doped MCT) or one (for antimony-doped MCT) stages with different characteristic relaxation times. This relaxation law corresponded to chemical-kinetic equation of the first order:

$$dn/dt = -k_1 n, \quad (15)$$

where  $k_1$  is reaction rate constant,  $n$  is concentration of donor defects formed under IE. The relaxation process is then related to disintegration of the donor defects. For sample doped with arsenic, fitting of experimental data yielded the following relation:

$$n = 3 \times 10^{16} \cdot \exp(-t/\tau_1) + 1.2 \times 10^{16} \cdot \exp(-t/\tau_2) + 4.2 \times 10^{15} \cdot \exp(-t/\tau_3) + 3 \times 10^{15}, \quad (16)$$

where  $\tau_1 = 50$  min,  $\tau_2 = 2500$  min,  $\tau_3 = 70,000$  min. For the antimony-doped sample, because of very small relaxation time, only the final stage of relaxation (a 'tail') was observed, therefore fitting was rendered useless. In any case, these data proved that donor defects formed under IE in antimony-doped MCT were much less stable than those in arsenic-doped MCT.

The electron concentration straight after IE  $n_{77i} \approx (2-4) \times 10^{16} \text{ cm}^{-3}$  in the bulk  $n$ -layer of arsenic-doped samples (Fig. 9) was close to  $p_{77}$  and  $N_{\text{As}}$  (as defined with secondary-ion mass-spectroscopy, SIMS) in the sample before IE. Electron concentration after relaxation  $n_{77f}$  in the bulk layer was much lower,  $\sim(2-3) \times 10^{15} \text{ cm}^{-3}$ , and could be related to background donor doping typical of ISOVPE. In Sb-doped sample,  $n_{77i} = 3 \times 10^{15} \text{ cm}^{-3}$  was much lower than  $p_{77}$  before IE ( $\sim 1.8 \times 10^{16} \text{ cm}^{-3}$ ) and indeed lower than Sb concentration determined with SIMS ( $\sim 7 \times 10^{16} \text{ cm}^{-3}$ ). This, again, was indicative of possible relaxation of donor defects during IE, confirming low stability of these defects. The value of  $n_{77f} \approx 1.5 \times 10^{15} \text{ cm}^{-3}$  in this material could be related either to background doping or to high  $n_i$  in the samples with low  $x$  ( $\sim 0.18$ ).

Later, the authors of Refs. [15,69–73] conducted numerous experiments on CTC in arsenic-doped MCT grown with MBE and MOCVD and subjected to IE. The basic properties of the converted layers in these samples were similar to those described above; the only difference was related to the initial stage of relaxation and

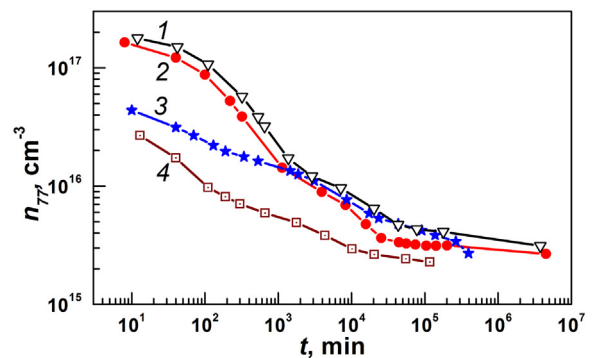
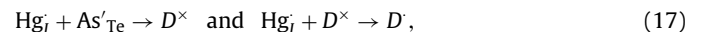


**Fig. 10.** Post-IE relaxation of  $n_{77}$  in MBE-grown arsenic-doped MCT (curves 1 and 2). Curves 3 and 4 show relaxation in arsenic-doped MCT with similar  $x$  grown with ISOVPE and MOCVD, respectively [72,73].

was caused not by the presence of arsenic, but rather by some neutral defects described below. Typical of arsenic-doped MCT appeared to be the absence of re-conversion back to  $p$ -type under storage at 300 K for as long as 10 years (Fig. 10) [72]. A trend of re-conversion back to  $p$ -type in ISOVPE-grown arsenic-doped MCT film was observed at  $T > 100^\circ\text{C}$  during isochronous annealing in the temperature range 20–140 °C with step 20 °C and duration of each stage 30 min [67].

The mechanism of CTC in arsenic- and antimony-doped  $p$ -MCT was proposed by the authors of Refs. [28,64]. The authors of Ref. [28] suggested that under IE, singly charged interstitial mercury formed donor complexes with background arsenic according to the reactions:



where  $D^\times$  stands for neutral complex.

The detailed consideration of the mechanism of CTC in As(Sb)-doped  $p$ -MCT was given in Refs. [64–66]. It was based on the assumption that in the process of diffusion, doubly charged  $\text{Hg}_l^{++}$  atoms react with singly charged As (or Sb) acceptors, which are located in the anion sublattice ( $X'_{\text{Te}}$ ). As a result of this reaction, singly charged donor complex  $D^-$  is formed:



The corresponding mass action law is:

$$[\text{Hg}_l^+] \cdot [X'_{\text{Te}}] = K_X [D^-], \quad (19)$$

where  $K_X = K_0 \cdot \exp(-\Delta H_{cX}/k_B T)$  is the equilibrium constant ( $K_0 \approx N_0$  is a node density in the metal sublattice), and  $\Delta H_{cX}$  is enthalpy of the complex formation. Equation (19) should be supplemented by a condition of the existence of a permanent amount of the V-group element  $[X]_\Sigma$  dissolved in the crystal. From these equations, an expression for donor center concentration follows:

$$[D^-] = \frac{[\text{Hg}_l^+]}{[\text{Hg}_l^+] + K_X} [X]_\Sigma. \quad (20)$$

The condition of the formation of donor complexes  $[\text{Hg}_l^+] \gg K_X$  follows straight from the Eq. (20). At 300 K under typical IE conditions ( $[\text{Hg}_l^+] \sim 10^{14} \text{ cm}^{-3}$  [43]) the V-group acceptor dopants should be bound in complexes with  $\text{Hg}_l^+$  at  $\Delta H_{cX} > 0.6 \text{ eV}$ . The values of  $\Delta H_{cX}$  were assessed for arsenic- and antimony-doped material as  $1 \pm 0.1 \text{ eV}$  and  $0.8 \pm 0.2 \text{ eV}$ , respectively. These estimations meant a high probability of the complex formation under IE.

The reaction of the formation of the donor complex ( $X'_{\text{Te}} - \text{Hg}_l^+$ ) is similar to that of annihilation of  $\text{Hg}_l^+$  and  $V''_{\text{Hg}}$ , yet differs from the latter in that a new chemical bond is formed, so a certain potential

barrier ( $E_{ax}$ ) should be overcome. Thus, the constant  $k_X$  of the rate of the reaction of complex formation should be written as:

$$k_X = k_{0X} \exp(-E_{ax}/k_B T), \quad (21)$$

where  $k_{0X} = 4\pi r_X(D_I + D_X) = 4\pi r_X D_I$ ,  $D_X$  is diffusion coefficient of the acceptor dopant and  $r_X$  is a capture radius, which for oppositely charged centers  $r_X \approx r_D$ , where  $r_D$  is a screening radius. As for As and Sb  $D_X$  is really small, it can be regarded that  $D_X = 0$ . Thus,  $k_{0X} \approx k_F$ , which means that conversion depths should be similar in vacancy- and acceptor-doped MCT subjected to IE with all other conditions being the same. Among other things, this is due to the same values of  $[Hg_i^-]_S$  in both cases.

The conversion mechanism proposed in Refs. [64–66] agrees with all the experimental data. Electron concentration  $n_{77i}$  in arsenic-doped samples (except for MBE samples) agrees well with  $N_{As}$ , which means that it is indeed defined by  $As'_Te - Hg_i^-$  donor complex concentration. The weaker stability of the complexes in MCT doped with Sb can be explained by the value of  $\Delta H_{cSb}$  being too close to the critical value of  $\Delta H_{cX} = 0.6$  eV, and this easily explains the discrepancy between the  $n_{77i}$  and acceptor concentration in the Sb-doped samples measured before IE.

The proposed CTC mechanism implies that after IE is stopped and  $Hg_i^-$  concentration decreases (due to diffusion of these atoms back to the surface) to a level that corresponds to the condition  $[Hg_i^-] \ll K_X$ , according to Eq. (20), the donor complexes begin to disintegrate. The kinetics of this process should correspond to the chemical-kinetic equation of the first order that has a solution in the form of the exponential law:

$$\tau_X = \frac{1}{k_X K_X} = \frac{1}{k_{0X} N_0} \exp\left(\frac{E_{ax} + \Delta H_{cX}}{k_B T}\right). \quad (22)$$

Estimations showed that at  $T = 300$  K,  $E_{ax} = 0.2$  eV,  $\Delta H_{cAs} = 1$  eV and  $\Delta H_{cSb} = 0.8$  eV, the disintegration time is  $\tau_X \sim 3105$  min and  $\tau_X \sim 150$  min for MCT doped with As and Sb, respectively. However, such relaxation mechanism should result in the complete re-conversion of the  $n$ -layer back into  $p$ -type, which was not observed in the experiment even after the samples were stored for more than 10 years (Fig. 10) [72]. This pointed out to the fact that in reality the relaxation process occurs in a more complicated way, possibly via formation of neutral complexes  $D^\times (D \rightarrow Hg_i^- + D^\times)$ , as was suggested in Ref. [28]. These neutral complexes are stable at 300 K.

According to Refs. [64–66], to achieve CTC in arsenic- or antimony-doped MCT, in contrast to vacancy-doped material, one should have  $[Hg_i^-] \gg K_X$  condition fulfilled. This requires a certain value of ion current density and sets a limit on this value. Under typical IE regimes ( $j = 0.1$ – $0.3$  mA/cm $^2$ ), this condition is easily satisfied. The existence of such condition was confirmed by the authors of Ref. [74] when they compared arsenic-doped samples subjected to IE to similar samples with anodic oxide (AO) annealed in air at 428 K for 20 min. Deep CTC was not observed for the latter sample, while in sample subjected to IE the CTC depth equaled  $\sim 6$   $\mu$ m. A vacancy-doped sample (with similar  $[V_{Hg}]$  and  $N_{As}$ ) after anodic oxidation and annealing demonstrated CTC depth of 10  $\mu$ m.

These facts agree with the above proposed CTC mechanism and conditions for the conversion. Under annealing of AO, CTC results from the diffusion of free mercury atoms that appear as a result of the oxidation and are forced to move to the border between the AO and the crystal. Concentration of  $Hg_i^-$  in this case cannot exceed its equilibrium value at the temperature of the annealing, which at  $T = 428$  K equals  $\sim 10^9$  cm $^{-3}$  [47]. At this temperature and at  $H_{cAs} \approx 1$  eV, the constant of the formation of the donor complex  $K_{As} \approx 10^{10}$  cm $^{-3}$ . Thus, the condition  $[Hg_i^-] \gg K_X$  is not satisfied, arsenic atoms remain in the form of  $As'_Te$  and no CTC is observed. In contrast to this, under IE,  $[Hg_i^-] \gg K_X$  is easily satisfied and deep CTC

is observed. For vacancy-doped MCT, no conditions are required and annealing of AO leads to deep CTC.

Let us note that CTC under IE was also observed in arsenic-doped MCT in Ref. [39]. Studied were LPE-grown  $p$ -MCT films with  $x = 0.23$  and  $0.28$ . The electron concentration after IE was equal to  $N_{As}$  (though relaxation of  $n_{77i}$  was not considered). The CTC depth  $d_j$  dependence on the thickness of the layer etched off with IE (which means, on the etching time) and on arsenic concentration looked like  $d_j \propto t^{0.9}$  and  $d_j \propto N_{As}^{-1}$ , respectively, which agreed with the kinetic mechanism of CTC. However, when studying  $d_j(N_{As})$ , the authors of Ref. [39] did not consider  $d_j(x)$  and directly compared the data acquired on samples with different composition, which makes the  $d_j \propto N_{As}^{-1}$  relation somewhat doubtful. It was shown also, that annealing of the IE-converted films at  $T = 120$  °C for 96 h brought the parameters of the films back to those of initial samples, similar to the data of Ref. [62]. The authors of Ref. [39] claimed that CTC mechanism was related to the formation of donor complexes according to the reaction  $Hg_i^- + As'_Te \leftrightarrow As'_TeHg_i^-$ . They, however, did not give any arguments supporting this idea, nor they referred to Refs. [28,64–66], where this mechanism had been already proposed and proven by that time.

## 2.7.2. Conductivity type conversion in Cu-, Ag- and Au-doped MCT

CTC in Au-doped LPE-grown  $p$ -MCT films under reactive IE was first reported on in Ref. [53] and was studied in more detail in Ref. [54]. A comparison was made of the effect of reactive IE in  $CH_4/H_2$  plasma on vacancy-doped ( $x = 0.23$ ;  $p_{77} = 1.2 \times 10^{16}$  cm $^{-3}$  and  $x = 0.31$ ;  $p_{77} = 7.4 \times 10^{15}$  cm $^{-3}$ ) and Au-doped ( $x = 0.23$ ;  $p = 1.2 \times 10^{16}$  cm $^{-3}$  and  $x = 0.31$ ;  $p = 9.3 \times 10^{15}$  cm $^{-3}$ ) films. Etching for 2 min removed a  $\sim 0.3$   $\mu$ m-thick layer. With the use of step-by-step chemical etching, CTC depth of 4  $\mu$ m was found in MCT with  $x = 0.23$  doped with Au and 1  $\mu$ m in other samples. With the use of quantitative MSA, electrons with low ( $2000$ – $3000$  cm $^2$ /(Vs)) and high ( $40,000$ – $80,000$  cm $^2$ /(Vs)) mobilities were identified in the converted  $n$ -layer, which was typical of the damaged  $n^+$ -layer and the bulk  $n$ -layer, respectively. For low-mobility electrons  $\mu_n$  did not depend on temperature in 30–300 K range, while temperature dependence of  $\mu_n$  for high-mobility electrons was typical of uncompensated MCT with appropriate  $x$ . At that,  $\mu_{n77}$  in Au-doped MCT was 1.5 to 2 times higher than that in the vacancy-doped material. Surface concentration of low-mobility electrons at 77 K equaled  $8 \times 10^{12}$  cm $^{-2}$  in all the samples. The average concentration of high-mobility electrons at 77 K in Au-doped MCT with  $x = 0.23$  ( $\approx 3 \times 10^{15}$  cm $^{-3}$ ) was an order of magnitude lower than the concentration of Au. For the vacancy-doped material, this concentration reached  $8 \times 10^{15}$  cm $^{-3}$ , which was much higher than the value reported on by other authors [12]. However, the authors of Ref. [54] did not consider possible relaxation of the parameters after IE.

In relation to the mechanism of CTC, the authors of Ref. [54] made the following conclusions. Diffusion-like profile of the electron concentration in the converted layer, in their opinion, was indicative of the fact that CTC was related to diffusion of some donor impurities from the surface (the origin of those was not specified). This was also confirmed, as thought the authors of Ref. [54], by the fact that concentration of high-mobility electrons after IE significantly exceeded that of residual donors ( $\sim 3 \times 10^{14}$  cm $^{-3}$ , which, in fact, contradicted their own data obtained on the vacancy-doped samples). However, as the electron concentration in the converted layer was lower than  $N_{As}$ , the authors of Ref. [54] still believed that CTC mechanism was related to neutralization of Au dopant and diffusion of some donor impurities.

The authors of Ref. [75] considered formation of  $n$ -region in vertically-integrated photodiodes with circular  $p$ - $n$  junctions (loop-hole photodiodes) with the use of IE and ion implantation in

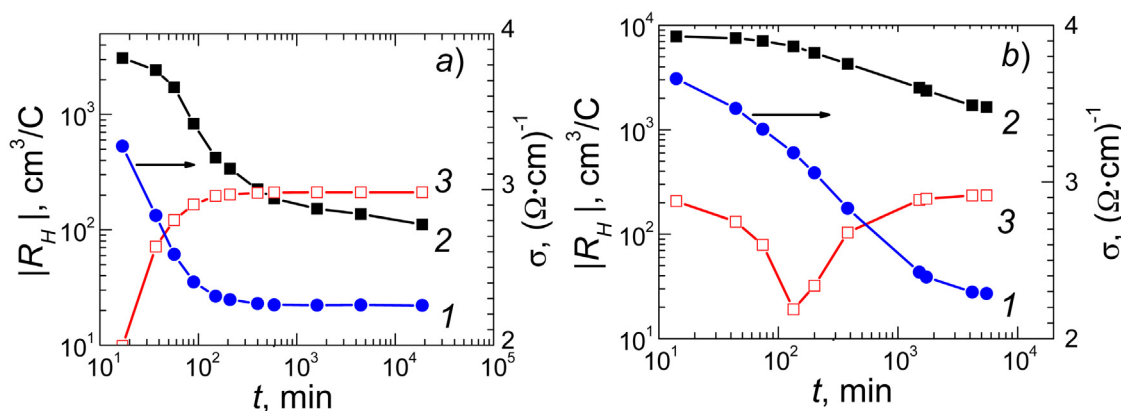


**Fig. 11.** Time dependence of integral values of conductivity (curve 1) and the Hall coefficient (2, 0.05 T; 3, 1.0 T) (77 K) after IE of Cu-doped p-MCT during storage at  $T=293\text{ K}$  (a) and  $T=273\text{ K}$  (b). (a) 2,  $R_H < 0$ ; 3,  $R_H > 0$ ; (b) 2,  $R_H < 0$ ; 3,  $R_H$  with sign inversion (after [78]).

Au-doped *p*-MCT co-doped with In ( $\sim 3 \times 10^{14}\text{ cm}^{-3}$ ). They related formation of  $n^+$ -*n* regions in photodiodes with generation of  $\text{Hg}_I$  which expelled Au atoms from metal sublattice sites. Part of these Au atoms, in their opinion, diffused laterally and defined the position of *n*-*p* junction with carrier concentration in *n*-region defined by that of indium. No more data were available in Ref. [75], nor did the authors give references to any other works.

IE-related CTC in MCT doped with Ag, Na, Cu and Au was mentioned in Ref. [76], and it was stated that in all cases the conversion depth was the same. However, Ref. [76] does not provide any data illustrating these observations, references to other works are not given either.

The detailed and consistent studies of IE-induced (500 eV Ar ions) CTC in Cu-Ag and Au-doped *p*-MCT ( $x=0.21\text{--}0.23$ ) were performed in Refs. [77–79]. MCT samples with  $n_{77} \sim 3 \times 10^{14}\text{ cm}^{-3}$  were cut from bulk crystals and doped via depositing metallic films on their surface and annealing them in saturated mercury vapors at 573 K for 72 h. After doping, samples acquired *p*-type with  $p_{77} = (1.5\text{--}6) \times 10^{16}\text{ cm}^{-3}$  (depending on the dopant), which was indeed defined by the dopant, as vacancies in the samples were eliminated. Hole mobility at 77 K after doping equaled 300–500 cm<sup>2</sup>/(Vs). As was shown in Ref. [77], IE caused deep CTC in Cu-, Ag- or Au-doped *p*-MCT with formation of a typical  $n^+$ -*n*-*p* structure. To make the study of the properties of bulk *n*-layer simpler, straight after IE the samples were subjected to chemical etching in Br<sub>2</sub> + HBr, which removed the damaged  $n^+$ -layer. Post-IE relaxation in the samples was studied at  $T=293\text{ K}$  and 273 K. Concentration profiles were determined with differential Hall-effect measurements (with step-by-step chemical etching) on the samples that relaxed at 293 K.

Fig. 11 shows typical relaxation curves for samples doped with Cu. Discrete MSA showed [78], that storage at 293 and 273 K of samples with removed damaged layer caused decrease in the amplitude of the peak corresponding to high-mobility electrons. This was indicative of the decrease in the concentration of the IE-induced donor centers which, therefore, were unstable.

Comparison of the relaxation curves recorded at 293 and 273 K (Fig. 11) shows that relaxation is thermally activated. Similar dependencies were observed for Ag- and Au-doped samples, and characteristic relaxation times depended on the dopant, which was indicative of different degrees of the stability of the donor centers. Relaxation of  $n_{77}$  in the bulk *n*-layers as determined from the original experimental data collected at storage temperature 273 K with the use of discrete MSA is shown in Fig. 12. The value of  $n_{77i}$  for all the samples agreed well with the concentration of introduced dopants. Relaxation of  $n_{77}$  was exponential and had two stages. It

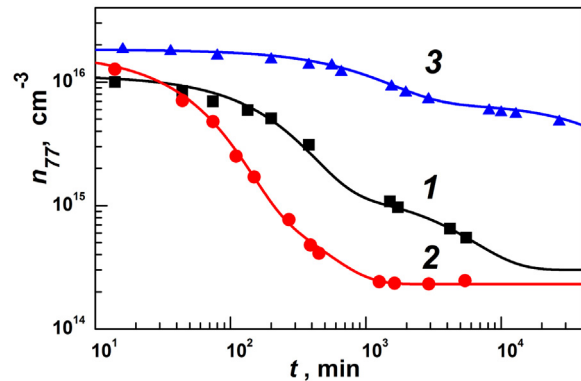


**Fig. 12.** Relaxation of  $n_{77}$  of the bulk converted layer at 273 K for Cu- (curve 1), Ag- (2) and Au-doped (3) *p*-MCT. Points show experimental data, lines are exponential fitting curves (after [77]).

reflected chemical-kinetic equation of the first order (Eq. (15)), and was related to disintegration of donor centers induced with IE.

Assuming that reciprocal characteristic relaxation time  $1/\tau$  depended on the temperature according to the Arrhenius law, it was found [77]:

$$\begin{aligned} \tau_{2\text{Cu}} &= 3.2 \times 10^{-8} \exp(0.632 \text{ eV}/k_B T_r) \text{ s;} \\ \tau_{2\text{Ag}} &= 5.4 \times 10^{-7} \exp(0.577 \text{ eV}/k_B T_r) \text{ s;} \\ \tau_{2\text{Au}} &= 1.5 \times 10^{-6} \exp(0.555 \text{ eV}/k_B T_r) \text{ s.} \end{aligned} \quad (23)$$

As can be seen, activation energies  $E_{a2}$  for all three dopants were similar, while in general relaxation was much slower in Au-doped sample.

Relaxation of these samples at 293 or 273 K did not lead to re-conversion back from *n*- to *p*-type [77]. For Cu- and Ag-doped samples, the bulk converted layer retained *n*-type with  $n_{77f} \approx 2 \times 10^{14}\text{ cm}^{-3}$ , which was close to background donor doping level. In Au-doped sample,  $n_{77f} \approx 2 \times 10^{15}\text{ cm}^{-3}$  exceeded the latter, which was probably due to incomplete relaxation in the course of the measurements. Isochronous annealing (after storage at 273 K) lead to decrease in  $n_{77}$  (after 80 °C annealing stage) and eventually to re-conversion back into *p*-type at  $T \geq 120\text{ }^\circ\text{C}$ .

A consistent mechanism of CTC in ion-etched Cu-, Ag- and Au-doped MCT was proposed in Refs. [77,78]. All the experimental data on the topic suggested that Cu, Ag and Au are also (similar to As and Sb) able to interact with  $\text{Hg}_I$ , which results in changes in the charge

state of the dopants. Most likely, CTC in this case is caused by the reaction:



where  $M'_{\text{Hg}}$  is an acceptor,  $M_I$  is a donor,  $M$  stands for Cu, Ag or Au. This reaction corresponds to mass action law:

$$[\text{Hg}_I^{\cdot}][M'_{\text{Hg}}] = K_{rM}[M_I], \quad (25)$$

where  $K_{rM}$  is the equilibrium constant. Considering that  $[M'_{\text{Hg}}] + [M_I] = N_M$ , where  $N_M$  is the total concentration of the dopant, from Eq. (25) we obtain:

$$[M_I] = \frac{N_M[\text{Hg}_I^{\cdot}]}{[\text{Hg}_I^{\cdot}] + K_{rM}}. \quad (26)$$

Eq. (26) gives a condition for the formation of donor centers involving Cu, Ag or Au:  $[\text{Hg}_I^{\cdot}] \gg K_{rM}$ , which is similar to that in As- or Sb-doped MCT. Thus, according to Refs. [77,78], CTC in Ag-, Cu- or Au-doped MCT under IE is possible if  $K_{rM}$  is not too large. As discussed earlier, CTC under IE can be achieved at  $K_{rM} \ll 10^{14} \text{ cm}^{-3}$ , and estimations made in Refs. [77,78] showed that for Cu-doped MCT this condition is achieved at any  $E_{m\text{Cu}}$  (which is the dopant migration energy). For Au- and Ag-doped MCT, CTC is possible at  $E_{m\text{Ag}}$  (or  $E_{m\text{Au}}$ ) > 0.2 eV, which is still achievable, yet sets certain limits on IE parameters. In any case, CTC in I-group acceptor-doped MCT requires (similar to V-group acceptor-doped material) certain values of ion current density, which contrasts it to vacancy-doped MCT.

Typical characteristic time of transfer of  $M'_{\text{Hg}}$  into  $M_I$  can be assessed as  $\tau_{rIM} = 1/(k_{rM}[\text{Hg}_I^{\cdot}])$ , where  $k_{rM}$  is the reaction rate constant [78]. Considering typical parameters,  $\tau_{rIM} \sim 10^{-2} \text{ s}$ , which is much less than IE time ( $t \sim 10^3 \text{ s}$ ) and suffices for CTC. Thus, most probable mechanism of CTC in I-group acceptor-doped MCT under IE is diffusion of  $\text{Hg}_I^{\cdot}$  with kicking dopant atoms from cation sublattice (where they acted as acceptors) into interstitial position (where they act as donors), provided  $K_{rM} \ll [\text{Hg}_I^{\cdot}]$ . This mechanism implies equal CTC depth in Cu-, Ag- and Au-doped MCT and vacancy-doped MCT (Fig. 3), as well as similarity between  $n_{77i}$  in the converted layer and acceptor concentration in the initial sample, which agrees with experimental data quite well.

This mechanism surely implies post-IE relaxation, and according to Eq. (26), when  $[\text{Hg}_I^{\cdot}] \ll K_{rM}$  dopant atoms should move back to their initial positions in the cation sublattice with characteristic time  $\tau_{rrlx} = 1/(k_{rM}K_{rM})$ . However, estimations for  $\tau_{rrlx}$  made in Refs. [77,78] differed from experimental  $\tau_{2M}$  values. Also, if one accepts this model of relaxation, it becomes difficult to explain the lack of re-conversion back from  $n$ -type into  $p$ -type. Therefore, there should be other processes that slow down the re-conversion or hinder it completely. According to Refs. [77,78], most likely reason for this phenomenon is the disintegration of the formed solid solution, as the maximum solubility of  $M_I$  in MCT under at 300 K is much lower than  $10^{16} \text{ cm}^{-3}$  [80]. As the migration energy is large,  $\tau_{rrlx}$  is large, too. Also, because of the disintegration, concentration of  $M_I$  in the converted layer gets much lower than  $N_M$ . Because of this, the rate of  $M'_{\text{Hg}}$  formation also becomes low, and re-conversion is not observed. On the other hand, in the bulk of the sample concentration of the solution is much lower than in a saturated solution, thus for some time after IE the flux of  $M_I$  is directed from the converted layer into the bulk of the crystal, which does not favor re-conversion either. At that, conductivity type would be defined by background impurities, which agrees with the experimental data. With time, inclusions should dissolve as a result of the transfer of  $M_I$  into  $M'_{\text{Hg}}$ , and then re-conversion becomes possible, as was shown in Ref. [72] for Ag-doped MCT.

## 2.8. Stability and relaxation of parameters of MCT modified with ion etching

Stability of the properties of  $p(n)$ -MCT layers converted (modified) with IE is very important considering the fact that this method is widely used for fabrication of photodetectors. The authors of Ref. [28] were the first to observe relaxation of electrical parameters of  $n$ -layers formed with IE in vacancy-doped MCT. Relaxation has been followed for several weeks while the samples were stored at the room temperature. We shall call this relaxation (or stability) a ‘short-term’ one ( $\sim 10^5 \text{ min}$ ) in contrast to long-term relaxation (stability) that can be followed for several years.

Stability of  $n-p$  structures formed with IE was first studied in Ref. [24]. The position and shape of  $p-n$  junction were measured by EBIC straight after IE and three months later (the sample was kept in air at the room temperature) with no difference observed.

In some papers, the effect of thermal annealing on the properties of modified/converted MCT layers was studied. In Ref. [29], it was shown that low-temperature annealing at  $75-80^\circ\text{C}$  for 24–170 h of  $n^+ - n$  structure fabricated on the basis of  $n$ -MCT ( $x=0.215$ ,  $n=1 \times 10^{15} \text{ cm}^{-3}$ , carrier lifetime  $\tau \sim 3 \mu\text{s}$ ) with low degree of compensation and subjected to IE ( $E=100 \text{ eV}$ ,  $j=0.5 \text{ mA/cm}^2$ ,  $t=60 \text{ min}$ ) led to slight increase in electron concentration and hardly affected concentration profile and mobility values. The carrier lifetime, however, did change after annealing: its value got restored back to  $0.2 \mu\text{s}$  as compared to  $1-2 \text{ ns}$  straight after IE. Annealing at  $70^\circ\text{C}$  for 48 h of ion-etched  $n^+ - n$  structure, which was based on strongly compensated  $n$ -MCT, after removing  $5 \mu\text{m}$ -thick layer with chemical etching, reduced electron concentration by the factor of 2 and led to increase in mobility and carrier lifetime (all measured at 77 K). The authors of Ref. [29] concluded that such annealing led to almost complete annihilation of defects in  $n^+$ -layer thus bringing its parameters to those of the bulk  $n$ -layer.

In Ref. [23], straight after IE it was not possible to detect carrier lifetime signal. After a  $\sim 5 \mu\text{m}$ -thick layer was removed with chemical etching, the measured lifetime exceeded that typical of the initial sample. After annealing at  $185^\circ\text{C}$  for 12–18 h, the lifetime decreased.

The authors of Ref. [81] studied the effect of thermal annealing under reduced mercury pressure on ion-etched (in Ar or  $\text{H}_2$  plasma) vacancy-doped  $p$ -MCT ( $x=0.23$ ;  $p_{77}=(5-10) \times 10^{15} \text{ cm}^{-3}$ ). Straight after IE, a  $1 \mu\text{m}$ -thick surface layer was removed with chemical etching. It was discovered that annealing of the  $n$ -layer formed as a result of IE in  $\text{H}_2$  plasma, performed at  $150$ ,  $190$  or  $210^\circ\text{C}$  for 300, 20 and 0.3 h, respectively, led to full re-conversion back into  $p$ -type. For the layer that was converted into  $n$ -type in Ar plasma, full re-conversion back into  $p$ -type required longer annealings, which was explained by a thicker converted layer. The activation energy of the re-conversion process in both cases was determined to be  $E_a=0.99 \text{ eV}$  and was, therefore, close to  $\text{Hg}_I^{\cdot}$  diffusion activation energy ( $1.01 \text{ eV}$ ). It was concluded that the re-conversion process was determined by the diffusion of  $\text{Hg}_I^{\cdot}$ .

Thermal stability of  $n-p$  structures formed with IE in vacancy-doped  $p$ -MCT ( $x=0.21$ ;  $p_{77}=5.8 \times 10^{15} \text{ cm}^{-3}$ ) was studied also in Ref. [82]. The CTC depth was  $10 \mu\text{m}$ . After IE, the structures were annealed in air at  $85$ ,  $120$  and  $160^\circ\text{C}$  for 1, 2 and 4 h. It was shown that annealing at  $160^\circ\text{C}$  for 2 h caused full re-conversion back into  $p$ -type. Annealing at  $85^\circ\text{C}$  caused some minor changes in electrical parameters at its initial stage, yet further (for the next 4 h) these parameters remained stable. Annealing at  $T=120^\circ\text{C}$  resulted in gradual re-conversion of  $n$ -layer back into  $p$ -type. The authors of Ref. [82] related the process of re-conversion to the out-diffusion of  $\text{Hg}_I^{\cdot}$  and formation of  $V_{\text{Hg}}$  in the converted layer, as the effect of the diffusion of the vacancies could be disregarded. The annealing temperatures and times that were required for achieving re-conversion

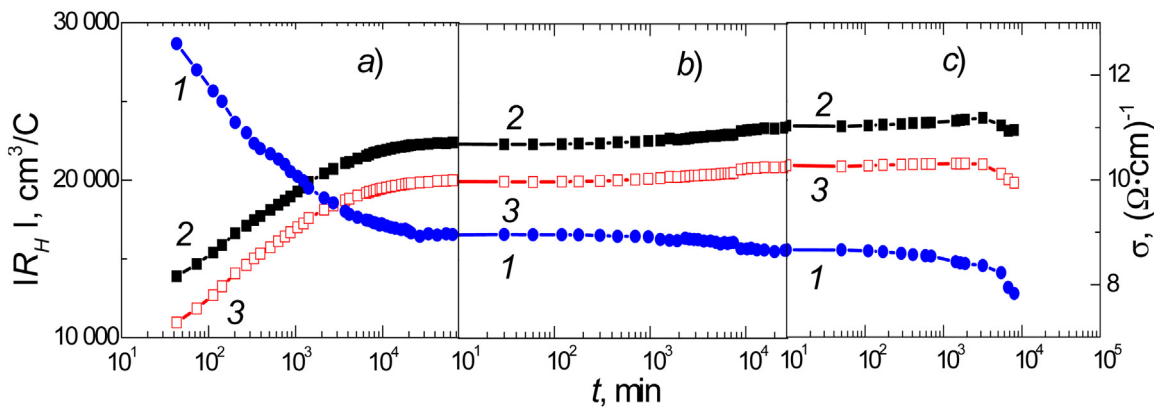


**Fig. 13.** Relaxation of integral conductivity (curve 1) and the Hall coefficient (2, 0.05 T; 3, 1.0 T,  $R_H < 0$ ) ( $T = 77$  K) during isothermal storage of IE-modified  $n$ -MCT structure with the damaged layer removed: (a), 20°C; (b), 50°C; (c), 75°C (after [68]).

in Ref. [82] were much lower than those in Ref. [81] and better suited general perception of the thermal stability of MCT.

Finally, the authors of Ref. [28] discovered relaxation of electrical parameters of IE-formed  $n$ - $p$  structures during the storage of the etched samples at 300 K. It was established that integral conductivity  $\sigma$  of the structures (as measured at 77 K) formed with reactive IE in  $H_2$  or Ar plasma in vacancy-doped  $p$ -MCT ( $x=0.21$ ;  $p_{77}=(1-4) \times 10^{16} \text{ cm}^{-3}$ ), decreased monotonically after IE in the course of the storage. After a few days,  $\sigma$  experienced saturation. Increasing the storage temperature up to 323 K lead to 5-fold acceleration of relaxation, so it was concluded that relaxation was a thermally activated process. The studies of the differential Hall effect showed that after the relaxation the converted layer retained  $n$ -type conductivity and  $\sigma$  was constant throughout the thickness of the layer. In accordance with the mechanism proposed in Ref. [28], relaxation of electrical parameters was caused by the disintegration of donor complexes formed during IE by  $Hg_I$  with background impurities, such as, e.g., arsenic.

Qualitatively the long-term stability of  $n^+$ - $n$  structures formed with IE in vacancy-doped LPE-grown  $p$ -MCT films ( $x=0.22$ ;  $p_{77}=2 \times 10^{16} \text{ cm}^{-3}$ ) was studied in Ref. [83]. A comparison was made between the parameters of  $n^+$ - $n$  structures formed with IE after long-term (10 years) and middle-term (5 months) storage of the samples at 300 K. The most important practical conclusion of this work was related to the fact that  $n^+$ - $n$  structure of the converted layer with low-mobility (damaged  $n^+$ -layer) and high-mobility (bulk  $n$ -layer) remained as such after 10 years of storage at the room temperature.

The authors of Ref. [68] showed that relaxation of electrical parameters in the course of storage at 300 K is typical of  $n^+$ - $n$  structures formed with IE. They used wafers cut from the bulk vacancy-doped  $p$ -MCT crystals doped from the melt with Se (~1 at.%) or co-doped with In ( $N_D \approx 3 \times 10^{15} \text{ cm}^{-3}$ );  $n$ -type wafers cut from crystals doped with In ( $N_D=(2-4) \times 10^{14} \text{ cm}^{-3}$ ) and ISOVPE  $p$ -MCT films doped with As. Fig. 13 shows experimental data for the IE-modified sample with  $n$ -type conductivity.

The basic relaxation regularities appeared to be similar for ion-etched samples with initial  $p$ - and  $n$ -type conductivity. It was shown, via observation of integral conductivity behavior, that after relaxation is completed, the converted/modified layer remains in place. However, the authors of Ref. [68] established different character of relaxation in the samples with and without damaged layer, which was indicative of different nature of donor centers in the damaged  $n^+$ -layer and bulk  $n$ -layer.

Analysis of the parameters of the diffusion of  $Hg_I$  performed on the basis of the data presented in Ref. [47], showed that at  $T \leq 75^\circ\text{C}$  and  $t < 10^5$  min the diffusion of  $Hg_I$  caused by its evap-

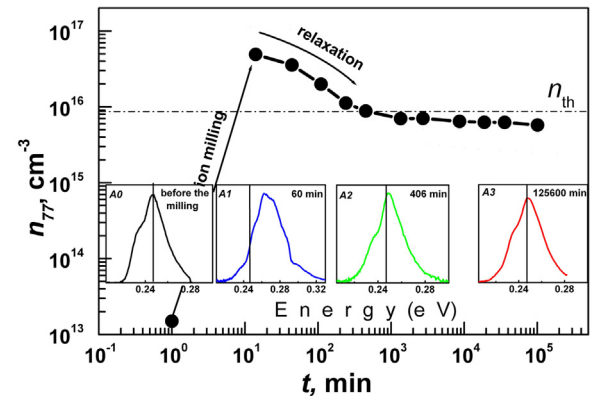


**Fig. 14.** Relaxation of electron concentration in IE-modified ‘bulk’ layer of the MBE-grown  $n$ -MCT with  $x \approx 0.3$  (graph) and the position of the band-edge photoluminescence band (insets) (after [84]).

oration from a homogeneous crystal into vacuum cannot possibly cause the increase in  $[V_{Hg}]$  greater than that at the tellurium border of the homogeneity region,  $[V_{Hg}]_{Te} < 10^{13} \text{ cm}^{-3}$ . Therefore, post-IE relaxation at 300 K is most likely caused by the decomposition of the donor centers, which were formed under IE in the damaged  $n^+$ -layer and bulk  $n$ -layer, as was suggested in Ref. [28] and was directly shown in Ref. [68]. Later, it was shown that under IE  $Hg_I$  can form donor complexes with some neutral defects (possibly, tellurium nanocomplexes) [15]. At that, let us underline the fact that the effect of post-IE relaxation in  $n^+$ - $n$  structures at 300 K was confirmed in numerous experiments via the Hall effect measurements by only two groups of researchers [28,68] and was studied in detail only by the authors of this review. To the best of our knowledge, no other research group has ever reported on this subject.

The authors of Ref. [84] confirmed the existence of relaxation, which had been already known at the time from the results of electrical measurements, by studying the blue-shift of band-edge photoluminescence at 84 K in ion-etched MBE-grown  $n$ -MCT ( $x \sim 0.3$ ) (Fig. 14).

The blue-shift was caused by the Burstein–Moss effect, when electron concentration exceeded a certain ‘critical’ level; reflecting the crossing of the conductivity band bottom by the Fermi level. The insets in Fig. 14 present the spectra of the MCT film measured before IE and during the relaxation (60, 406, and 125,600 minutes after the treatment, respectively). Vertical line in each spectrum presents the position of the maximum of the luminescence band was blue-shifted by ~17 meV from that of the original

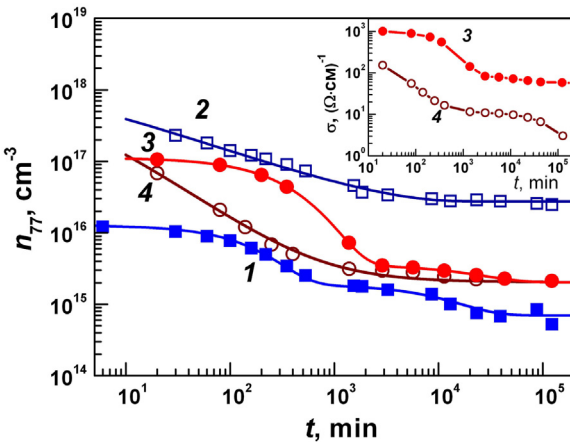


**Fig. 15.** Relaxation of  $n_{77}$  during isothermal aging at  $T=293\text{ K}$  for  $n\text{-}p$  structures in sample with removed damaged layer (curve 1) and  $n^+\text{-}n$ -structure in MBE-grown film without graded-gap surface layer (curve 3), for  $n^+$ -damaged layer (curve 2) and MBE-grown film with graded-gap surface layer with  $x_y \sim 0.56$  (curve 4) [49,58,86]. Inset shows relaxation of integral conductivity in MBE-grown samples with  $x_a \approx 0.22$  and  $x_y = 0.22$  (curve 3) and  $x_y = 0.56$  (curve 4).

spectrum. Four hundred minutes later the shift was  $\sim 3\text{ meV}$  and it slightly decreased over the following 125,600 min. As follows from Fig. 14, the appearance of the blue-shift in the luminescence band of ion-etched sample coincides with the increase of  $n_{77}$  due to the formation of the IE-induced defects. The threshold electron concentration  $n_{th}$  causing the Fermi level to enter the conduction band, as assessed by numerically solving an appropriate electro-neutrality equation for MCT with  $x=0.30$  at 84 K, is shown in Fig. 14 by the horizontal dash-dotted line. It is seen that the spectrum recorded straight after IE was indeed that of a degenerated sample ( $n_{77} \gg n_{th}$ ). The calculated electron concentration corresponding to a  $\sim 17\text{ meV}$  blue-shift was  $\sim 4 \times 10^{16}\text{ cm}^{-3}$ , being in a good agreement with the value of  $n_{77}$  measured at that point of relaxation. The other spectra were recorded when the  $n_{77}$  decreased below the threshold value, and no pronounced shift of the band was observed. The authors of Ref. [85] observed a similar effect; they, however, did not specify when exactly their spectra were recorded after IE, which does not allow for interpreting their data in the accurate way.

The studies of the mechanisms of conductivity and post-IE relaxation in various layers of  $n^+\text{-}n$  structure formed in vacancy-doped  $p\text{-MCT}$  were conducted in Refs. [49,58,86]. In particular, in Refs. [58,86] studied were identical single-crystal samples ( $x=0.205$ ;  $p_{77}=7.0 \times 10^{15}\text{ cm}^{-3}$ ), where the first sample straight after IE was subjected to chemical etching ( $\text{Br}_2 + \text{HBr}$ ) for removing  $\sim 4\text{ }\mu\text{m}$ -thick layer from the surface (including damaged layer), while the second sample was kept intact. In Refs. [49,58], a report was given on IE of MBE-grown  $p\text{-MCT}$  structures with graded-gap WBPLs ( $\sim 1.7\text{ }\mu\text{m}$ ) with composition at the surface  $x_y=0.22, 0.35, 0.48$  and  $0.56$ , respectively, yet with equal  $x_a \approx 0.22$ .

Fig. 15 shows the relaxation of  $n_{77}$  in IE-converted bulk  $n$ -layer measured during isothermal aging at  $300\text{ K}$  for  $n\text{-}p$  structure in sample with removed damaged layer (curve 1) and  $n^+\text{-}n$ -structure in MBE-grown film without graded-gap surface layer, where the conversion took place throughout the whole ( $10.8\text{ }\mu\text{m}$ ) thickness of the structure (curve 3). Also, similar curves are given for  $n^+$ -damaged layer (curve 2) and MBE-grown film with graded-gap surface layer with  $x_y \sim 0.56$  (curve 4).

For sample with removed damaged layer (curve 1) the MSA showed the presence of electrons of only one type, those of the bulk  $n$ -layer. For MBE-grown sample with  $x_a=x_y=0.22$  (curve 3) the electron concentration of the bulk  $n$ -layer was extracted with

MSA, and the dependence of  $n_{77}$  on the aging time  $t$  for both these samples was multi-exponential:

$$n = n_1 \exp(-t/\tau_1) + n_2 \exp(-t/\tau_2) + n_f. \quad (27)$$

As discussed above, such dependence is typical of the disintegration of donor centers (complexes) formed under IE as a result of interaction of  $\text{Hg}_I$  with I-(Cu, Ag, Au) and V-group (As, Sb) acceptors. This relaxation law corresponds to a simple kinetic Eq. (15).

Relaxation curves for the bulk of the converted layer have two important milestones: first is the initial electron concentration  $n_{77i}$ , measured 'straight after IE' (in reality,  $10\text{--}20\text{ min}$  later), and the second is  $n_{77f}$ , measured after saturation of the relaxation curve (which, as a rule, requires  $(1\text{--}2) \times 10^5\text{ min}$  of storage at  $300\text{ K}$ ). It was these values that were different for bulk-crystal sample (curve 1) and MBE-grown sample with  $x_a, x_y = 0.22$  (curve 3), which were obtained with different growth methods.

As can be seen, for bulk-crystal sample (curve 1),  $n_{77i} \sim 1.2 \times 10^{16}\text{ cm}^{-3}$ , which exceeded total concentration of background impurities in typical samples grown with this technology at "Pure Metals" factory (Svetlovodsk, Ukraine),  $(1\text{--}5) \times 10^{15}\text{ cm}^{-3}$ . After the relaxation  $n_{77f}$  was equal to  $\sim 7 \times 10^{14}\text{ cm}^{-3}$  and agreed well with the aforementioned background doping. For MBE-grown sample (curve 3),  $n_{77i}$  of  $\sim 10^{17}\text{ cm}^{-3}$  by two orders of magnitude exceeded the electron concentration in the as-grown  $n$ -type film (measured before the annealing performed to achieve CTC into  $p$ -type via vacancy doping). Considering the values of mobility in as-grown sample, the total concentration of background impurities did not exceed  $5 \times 10^{15}\text{ cm}^{-3}$ . After the relaxation,  $n_{77f}$  equaled  $\sim 2.5 \times 10^{15}\text{ cm}^{-3}$ , and, as was shown in many papers (see, e.g., [87]), was typical of MBE MCT grown on GaAs substrate. Also, as it was proven in Refs. [15,49,50,52,58,59,69,71], the value of  $\sim 10^{17}\text{ cm}^{-3}$  was typical of  $n_{77i}$  in all MBE-grown MCT films irrespective of the type of doping, substrate or specific epitaxy technology. As in the films before IE there were no electrically active impurities with such high concentration, it was suggested that in MBE-grown MCT an initially neutral defect was present. Interacting with  $\text{Hg}_I$  under IE, this defect forms donor centers with concentration  $10^{17}\text{ cm}^{-3}$ , similar to the case of acceptor-doped MCT. It was suggested that such defects can be represented by nanocomplexes of tellurium [15], especially considering non-equilibrium character of MBE of MCT, which typically proceeds under Te over-saturation. Possibly, similar nanocomplexes may exist in bulk crystals of MCT as well, even though they should have much lower concentration. The latter suggestion allows for explaining the fact that  $n_{77i}$  in bulk crystals slightly exceeded the concentration of background impurities, see curve 1 in Fig. 15.

According to Refs. [50,72], after the stage of short-term relaxation at  $300\text{ K}$ ,  $n_{77}$  remained stable during the long-term storage (6–10 years), as is shown in Fig. 16 for MBE-grown  $n\text{-MCT}$  ( $x \sim 0.2$ ) samples, un-doped and doped with indium in a wide concentration range ( $5 \times 10^{14}\text{--}10^{17}\text{ cm}^{-3}$ ). For nominally un-doped sample (curve 1) and that with indium concentration  $N_{\text{In}} \approx 5 \times 10^{14}\text{ cm}^{-3}$  (curve 2), electron concentration stabilized at  $n_{77f} \sim 2.5 \times 10^{15}\text{ cm}^{-3}$ , which corresponded to background donor doping  $N_{BD}$ . For samples doped with In with concentrations  $\sim 2.5 \times 10^{15}\text{ cm}^{-3}$  (curve 3) and  $\sim 1.3 \times 10^{16}\text{ cm}^{-3}$  (curve 4), electron concentration stabilized at the level  $n_{77f} \sim N_{BD} + N_{\text{In}}$ .

The results presented in this section unambiguously show that the mechanism of the relaxation of electrical parameters of the bulk  $n$ -layer in ion-etched  $p$ - and  $n$ -MCT is related to the disintegration of donor complexes and centers that  $\text{Hg}_I$  forms with background acceptors of I and V group, which represent basic uncontrolled impurities in MCT. Also,  $\text{Hg}_I$  may form similar complexes with some other residual impurities (O, C and H) and some neutral defects, such as tellurium nanocomplexes. As the chemical type of residual doping and the concentration of background impurities depend on

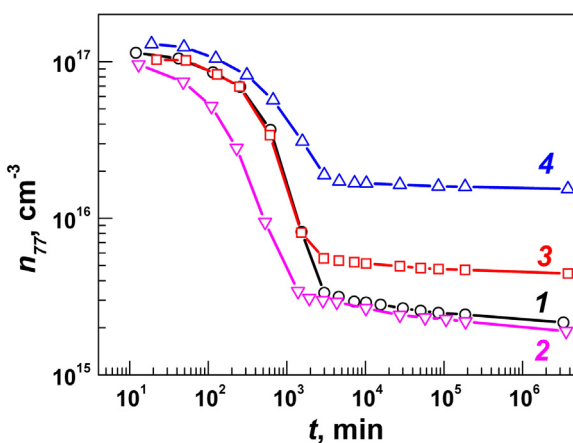


**Fig. 16.** Post-etching long-term relaxation of the electron concentration in the modified ‘bulk’  $n$ -layer of indium-doped  $n$ -MCT films: curve 1, un-doped film; 2,  $N_{\text{In}} \sim 5 \times 10^{14} \text{ cm}^{-3}$ ; 3,  $N_{\text{In}} \sim 10^{15} \text{ cm}^{-3}$ ; 4,  $N_{\text{In}} \sim 10^{16} \text{ cm}^{-3}$  [50,72].

the specific growth technology, it is this technology that eventually defines the character of relaxation in the given ion-etched sample. Also, it is shown that electron concentration in the bulk  $n$ -layer straight after IE is defined by the total concentration of residual donors, intentionally introduced donor dopants, and by the concentration of donor complexes and centers formed by  $\text{Hg}_l$  with acceptor impurities, and, possibly, with some neutral defects. After the relaxation and disintegration of the complexes and centers, the electron concentration in the bulk  $n$ -layer is determined by the total concentration of uncontrolled stable donors and intentionally introduced donor dopants (if any).

Electrical parameters of the damaged  $n^+$ -layer of  $n^+ - n$  structures formed with IE as dependent on storage time at 300 K are given in Fig. 15 for bulk crystal (curve 2) and MBE-grown sample with  $x_a \approx 0.22$  and  $x_y = 0.56$  (curve 4). To determine the characteristics of the  $n^+$ -layer in bulk crystal, the authors of Ref. [86] calculated and analyzed the difference between corresponding components of conductivity tensor for samples with and without  $n^+$ -layer during their storage at 300 K. Considering the identity of initial samples and IE regimes used, this difference indeed reflected the contribution of the  $n^+$ -layer. In MBE-grown sample with  $x_y \approx 0.56$ , IE resulted in  $n^+ - p$  structure with the thickness of  $n^+$ -layer of 2  $\mu\text{m}$ , without deep CTC.

As can be seen, for  $n^+$ -layers relaxation curves look very different as compared to those for the bulk  $n$ -layer. This is confirmed by a different character of the relaxation of integral conductivity for MBE-grown samples with  $x_y \approx 0.22$  and  $x_y = 0.56$  (curve 4) (inset in Fig. 15). The relaxation law at the initial relaxation stage could be described as:

$$n(t) = \frac{n(0)}{\sqrt{1 + kt}}, \quad (28)$$

where  $n(0) \approx 6 \times 10^{17} \text{ cm}^{-3}$ ,  $k \approx 0.005 \text{ s}^{-1}$  for sample 2 and  $n(0) \approx 3 \times 10^{17} \text{ cm}^{-3}$ ,  $k \approx 0.007 \text{ s}^{-1}$  for MBE-grown samples with  $x_y \approx 0.22$  and  $x_y = 0.56$ .

To explain the obtained results, the authors of Ref. [86] assumed that conductivity in  $n^+$ -layer was provided by donors formed via capture of  $\text{Hg}_l$  by neutral structural defects (dislocation loops). Condensation of  $\text{Hg}_l$  atoms and their transition back into the crystal matrix is favored not only by very high concentration, but also by very high mobility of this defect. Indeed, constant of  $\text{Hg}_l$  capture is of the order of  $4\pi r_{tr} D_l$ . In particular, for neutral capture centers, capture radius  $r_{tr}$  equals characteristic defect size  $a$ , and as  $D_l \sim 10^{-5} \text{ cm}^2/\text{s}$  at 300 K [27], at  $N_{tr} \sim 10^{18} \text{ cm}^{-3}$  characteristic capture time ( $1/kN_{tr}$ ) is only  $\sim 10^{-6} \text{ s}$ .

It was assumed that relaxation of donors in the damaged layer might proceed via re-structuring of a complex defect with the latter loosing its donor properties. For local re-structuring without emission of  $\text{Hg}_l$ , the most probable reaction of the lowest order in relation to the concentration of the centers:



where  $Tr$  stands for a trapping center. The kinetics equation for (29) is:

$$\frac{dN_0}{dt} = -k_0 n^2 N_0, \quad (30)$$

where  $k_0$  is reaction rate constant. Specifically, the reaction (29) was found to be three-molecular, provided that no other defects participated,  $N_0 \gg n_i$  and  $n = 2N_0$ . The solution of Eq. (30) is then reduced to (28), if it is assumed that  $k = 2k_0 N_0^2(0)$ . Fig. 15 (solid lines) shows the results of the fitting of experimental data performed with the use of Eq. (28). Good fitting is indicative of the fact that reaction according to Eq. (29) indeed takes place at the initial stage of the relaxation after IE.

On the basis of these results it was suggested that reaction Eq. (29) was associated with processes running in dislocation cores: a donor defect is formed when  $\text{Hg}_l$  is trapped by a dislocation core. In the process of relaxation, the defects are neutralized according to Eq. (29) and embed into the crystal lattice, causing the dislocation to shift. Correlation between typical relaxation times calculated using Eq. (28) and relaxation times of interstitial dislocation loops reported on in Ref. [56] provides strong confirmation to this interpretation.

### 3. Using ion etching for investigation of MCT defect structure

As basic patterns of the effect of IE on MCT and the properties of the etched material have been studied in much detail, it became possible to apply IE for studying MCT defect structure. The main postulates, which provide the basis for such studies, are:

- Extremely high concentration of non-equilibrium mercury interstitials ( $\sim 10^{14} \text{ cm}^{-3}$ ) in the source formed under IE (the equilibrium concentration at the room temperature is  $10^6 \text{ cm}^{-3}$ ) provides very high probability of the formation of donor centers and complexes comprising mercury interstitials and various dopants and defects (Cu, Ag, Au, As, Sb), certain neutral defects (possibly neutral Te nanocomplexes), dislocation loops;
- Donor centers and complexes formed under IE are unstable and after IE is stopped they start to disintegrate. The relaxation law for concentration of the electrons in the bulk converted (modified)  $n$ -layer is exponential with different characteristic times that depend on center type. For dislocation traps in the damaged  $n^+$ -layer, the law of relaxation is inverted square-root;
- The initial electron concentration after IE in the bulk converted/modified  $n$ -layer  $n_{77i}$  is equal to total concentration  $\sum N_d + \sum N_a + \sum N_{\text{neut}}$ , where  $\sum N_d$  is the total concentration of stable residual donors, native donor defects (antisite Te) and introduced donor dopants;  $\sum N_a$  is the total concentration of donor centers and complexes formed by  $\text{Hg}_l$  with acceptor dopants during IE, and  $\sum N_{\text{neut}}$  is the total concentration of donor centers and complexes formed by  $\text{Hg}_l$  with some electrically inactive defects.
- The electron concentration after relaxation in the bulk converted/modified  $n$ -layer is equal to the total concentration of donor dopants and centers,  $n_{77f} = N_{BD}$  (background donor concentration).

Further on we shall consider some examples of using IE for studying defects in MCT samples of various origins. The experimental set-up in all the works was the same. IE in DC Ar plasma was performed using an IB-3 (EIKO, Japan) etching system with  $\text{Ar}^+ E = 500 \text{ eV}$ ,  $j = 0.1\text{--}0.2 \text{ mA/cm}^2$ , and  $t = 10\text{--}20 \text{ min}$ . The temperature of the sample holder during the etching was kept at  $\sim 293 \text{ K}$  by means of cooling the holder with water. Post-IE relaxation was studied via periodic measurements of electrical parameters of the samples at 77 K while between the measurements the samples were kept in air at  $293 \pm 2 \text{ K}$ . First measurement was performed 10–15 min after IE. After short-term ( $(1\text{--}3) \times 10^5 \text{ min}$ ) relaxation was completed, part of the samples was stored for 6–10 years, and after that, the measurements were performed again. Electrical properties of the films were studied by measuring  $R_H$  and  $\sigma$  in magnetic field  $B$  of 0.01–1.5 T at  $T = 77 \text{ K}$  on square-shaped van der Pauw structures. The  $R_H(B)$  and  $\sigma(B)$  dependences were analyzed using discrete MSA [78].

### 3.1. Neutral defects in MCT

The possibility of the existence of certain neutral defects became a subject for discussion when the authors of Ref. [15] reported on the results of their studies of CTC in MBE-grown arsenic-doped structures with WBPL ( $x_a = 0.22$ ) (Fig. 10, curves 1 and 2). These and all other MBE structures discussed in this section (unless stated otherwise) were grown at Rzhanov Institute of Semiconductor Physics (ISP) (Novosibirsk, Russia) on (013) CdTe/ZnTe/GaAs (Si, ZnCdTe) substrates. Arsenic doping was performed from the effusion cell with high temperature at low substrate temperature  $T_{\text{sb}} \sim 165 \text{ }^\circ\text{C}$ . The as-grown films had  $n$ -type conductivity with the electron concentration  $n_{77(0)} \sim 8 \times 10^{15} \text{ cm}^{-3}$ . Thermal annealing ( $360 \text{ }^\circ\text{C}, 2 \text{ h}$ ) was used to activate the arsenic acceptor; this was followed by annealing at  $210 \text{ }^\circ\text{C}$  (24 h) under Hg saturation to fill the mercury vacancies that formed during  $360 \text{ }^\circ\text{C}$  annealing.

The arsenic concentration determined with SIMS was about  $N_{\text{As}} \sim 1.2 \cdot 10^{16} \text{ cm}^{-3}$ . After activation annealing, the samples became of  $p$ -type with  $p_{77} \approx 1 \times 10^{16} \text{ cm}^{-3}$ , which was indicative of 100% arsenic activation. According to the conversion mechanism discussed above, the concentration of donor complexes (reflected by  $n_{77i}$ ) in the bulk converted layer straight after IE should be equal to the acceptor dopant concentration ( $p_{77}$ ) in the initial sample. It was this trend that was observed, e.g., in ion-etched As-doped ISOVPE (curve 3 in Fig. 10) or MOCVD films (curve 4). But in some MBE-grown films the electron concentration in the bulk  $n$ -layers after IE was  $(1\text{--}2) \times 10^{17} \text{ cm}^{-3}$  and, therefore, could not be explained solely by interaction of  $\text{Hg}_I$  with the  $\text{As}_{\text{Te}}$  atoms. Thus, it was supposed that in MBE-grown MCT extra donor centers were formed, which resulted from the interaction of  $\text{Hg}_I$  with some intrinsic inactive defect [15]. This defect should have been neutral after growth/annealing (considering the parameters of the films before IE), and got activated upon IE, forming donor complexes with  $\text{Hg}_I$ .

Further studies showed that  $n_{77i} \sim (1\text{--}2) \times 10^{17} \text{ cm}^{-3}$  in the bulk converted/modified  $n$ -layer was the characteristic feature of all MCT epitaxial films grown with MBE at ISP. This concerns as-grown nominally un-doped  $n$ -type films and similar vacancy-doped (by annealing in He atmosphere)  $p$ -type films on GaAs, Si or ZnCdTe substrates; films doped with In and as-grown  $n$ -type films on GaAs substrates doped with As at low cracking temperature. It was also true for vacancy-doped MBE films grown on GaAs (211) substrates with the use of Riber-32p system. These results are summarized in Figs. 16–18. Let us note that for films with  $x_a \sim 0.3$  grown using different MBE technologies on GaAs(310) and GaAs(211) substrates,  $n_{77i}$  in the bulk converted/modified layer was lower,  $\sim 6 \times 10^{16} \text{ cm}^{-3}$ .

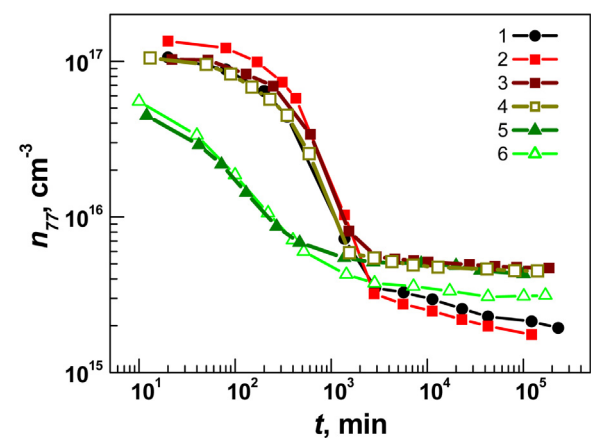


**Fig. 17.** Post-IE relaxation of the electron concentration in the 'bulk'  $n$ -layer for ISP MBE-grown MCT/GaAs films: curves 1 and 2, vacancy-doped  $p$ -type films with  $x_a \sim 0.22$  [49]; 3 and 4, as-grown In-doped  $n$ -type and similar vacancy-doped film with  $x_a \sim 0.22$  [50,88]; 5 and 6, as-grown un-doped  $n$ -type and similar vacancy-doped  $p$ -type films with  $x_a \sim 0.30$  [50,88].

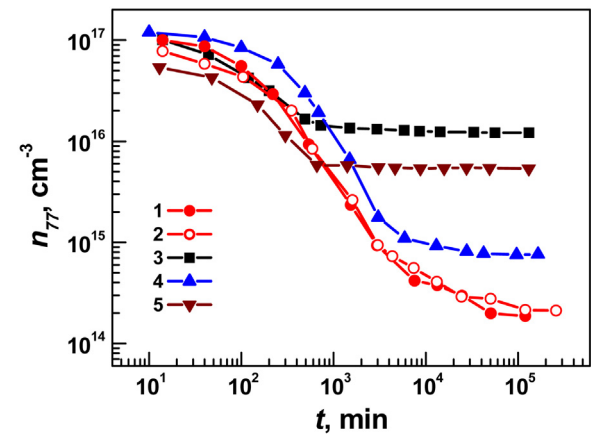


**Fig. 18.** Post-IE relaxation of the electron concentration in the 'bulk'  $n$ -layer for MBE-grown films: curves 1 and 2, as-grown un-doped  $n$ -type and similar vacancy-doped  $p$ -type ISP structures MCT/Si with  $x_a \sim 0.33$  [89]; 3, vacancy-doped with In co-doping ISP structure p-MCT/ZnCdTe with  $x_a \sim 0.23$  [90]; 4 and 5, MCT/GaAs(211) vacancy-doped with  $x_a \sim 0.22$  and  $x_a \sim 0.32$  grown in Riber-32p, respectively [90].

Thus,  $n_{77i}$  in the bulk converted/modified layer in MBE-grown samples does not depend on the substrate type, doping, post-grown annealing and specific technology, and is due to the specifics of MBE. Taking into account that MBE proceeds under substantial tellurium over-saturation, it was speculated that such defect may be Te-related, e.g., may represent Te nano-complexes.

A similar effect ( $n_{77i} \sim 10^{17} \text{ cm}^{-3}$ ) was also observed in LPE (performed from Te-rich melts) films grown on ZnCdTe substrates at JSC "Giredmet" (Moscow, Russia), Fig. 19 (curves 2–5), but was not observed in LPE films grown at JSC "Pure metals" (Svetlovodsk, Ukraine), Fig. 19, curve 1. For the latter,  $n_{77i}$  was only  $\sim 2 \times 10^{16} \text{ cm}^{-3}$ , similar to the case of MCT bulk crystals.

As is known, the problem of Te-related defects (tellurium macro-inclusions) existed at the early stages of MCT bulk crystal and LPE film technology. The problem was later solved with post-growth thermal annealings, which made the macro-inclusions dissolve in MCT matrix. This, however, does not imply that after such annealings nanocomplexes of tellurium may not remain. The results of Raman scattering study in films grown with LPE technology identical to that used for the growth of samples 2–5 in Fig. 19 showed the absence of Te macro-inclusions, but presence of Te nanocomplexes [91]. This indirectly confirms the results obtained

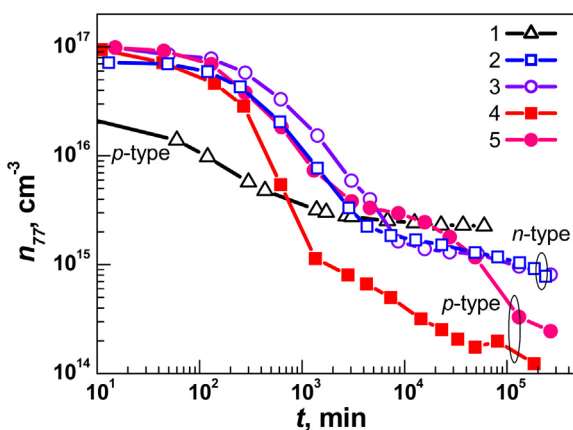


**Fig. 19.** Post-IE relaxation of the electron concentration in 'bulk' *n*-layer for LPE-grown films: curve 1, vacancy-doped *p*-type with  $x_a \sim 0.22$ ; 2 and 3, annealed into *n*-type with  $x_a \sim 0.20$ ; 4 and 5, vacancy-doped *p*-type with  $x_a \sim 0.20$  [51,90].

with IE. A similar tentative conclusion was made in Ref. [92] for MBE-grown MCT. Thus, using IE for studying defect structure of MCT films grown with MBE and some variations of LPE allowed for revealing certain neutral defects, which were tentatively identified as tellurium nanocomplexes.

### 3.2. Arsenic incorporation in molecular beam epitaxy-grown MCT

Arsenic is the acceptor dopant of choice for the growth of extrinsically doped *p*-type MCT layers, especially for photodetectors operating in the longer parts of the IR spectrum and at higher temperatures [63]. A problem related to arsenic doping in MBE-grown MCT is caused by the manner of As incorporation in the material [93]. As-grown films usually show *n*-type conductivity, as under typical MBE conditions arsenic is incorporated in MCT in a complicated way, interacting with intrinsic defects [94]. One of the major uncertainties is the exact knowledge of As position in the crystal lattice before and after post-growth thermal activation. To study this matter, the authors of Refs. [70,71] used IE.

Investigated were arsenic-doped MCT/GaAs ( $x_a \approx 0.21$ ) films grown with arsenic cracking [95]. Doping from the cracker cell was implemented with a flow of arsenic passing through a cracking zone. The flow rate was set by varying the source temperature  $T_{src}$ , with the fraction of  $\text{As}_2$  molecules in the flow controlled by the cracking zone temperature  $T_{cr}$ . Temperature of substrate  $T_{sb}$  during the growth of these samples was  $\sim 185^\circ\text{C}$ . All the as-grown films were of *n*-type conductivity. Samples grown at low  $T_{cr}$  ( $407$  and  $534^\circ\text{C}$ ) had low electron concentration ( $2 \times 10^{14}$  and  $2.2 \times 10^{15} \text{ cm}^{-3}$ , respectively) and could not be activated into *p*-type. Other samples, which were grown at the mediate ( $661^\circ\text{C}$ ) and high ( $781^\circ\text{C}$ )  $T_{cr}$ , had electron concentration in the range  $2 \times 10^{16}$ – $6.3 \times 10^{15} \text{ cm}^{-3}$ , and were successfully activated into *p*-type. IE and electrical measurements were performed on as-grown *n*-type samples and their counterparts activated into *p*-type. Fig. 20 presents the results of the study of post-IE relaxation in these samples.

The data presented in Fig. 20 can be interpreted using the hypothesis of the existence of Te-related defects in MBE-grown MCT. For As doping from an effusion cell with cracking at low cracking temperature ( $T_{cr} \sim 400$ – $500^\circ\text{C}$ ), arsenic in the flow is presented mainly in the form of tetramer molecule  $\text{As}_4$ . Taking into account  $n_{77(0)} \sim (2\text{--}20) \times 10^{14} \text{ cm}^{-3}$  (which was considerably lower than  $N_{\text{As}}$ ) and high value of  $n_{77i} \sim 10^{17} \text{ cm}^{-3}$  (which corresponds to the typical concentration of neutral Te complexes), it was proposed that under these conditions  $\text{As}_4$  did not interact with neutral Te nanocomplexes and was incorporated into the lattice in the form of

electrically inactive species. Under activation annealing the  $\text{As}_4$  was not activated, so the films kept initial *n*-type. Under IE,  $\text{Hg}_l$  formed donor complexes only with Te nanocomplexes, so the relaxation of  $n_{77}$  was associated with the disintegration of these complexes, as was the case for the un-doped sample (curve 1, inset).

For As doping with high cracking temperature ( $T_{cr} \sim 660$ – $780^\circ\text{C}$ ), arsenic in the flow was present mainly in the form of dimer molecule  $\text{As}_2$ . Taking into account the value  $n_{77(0)} \sim (6\text{--}20) \times 10^{15} \text{ cm}^{-3}$  and low value of  $n_{77i} \sim 4 \times 10^{16} \text{ cm}^{-3}$  (lower than typical concentration of neutral Te complexes), it was proposed that under these conditions  $\text{As}_2$  interacted with neutral Te nanocomplexes and got incorporated into the lattice in the form of donor complex  $\text{As}_2\text{Te}_3$ . Still, in the samples there could remain some neutral Te nanocomplexes. Under IE,  $\text{Hg}_l$  did not interact with donor complex  $\text{As}_2\text{Te}_3$ , so the weak relaxation of  $n_{77}$  was associated only with the disintegration of  $\text{Hg}_l$ -Te complexes (curves 1–3). For sample grown at highest arsenic effusion cell temperature (highest As flow) it was assumed that most of the excessive tellurium was bound into  $\text{As}_2\text{Te}_3$  donor complexes, which did not interact with  $\text{Hg}_l$ . As a result, after IE the relaxation of electron concentration was not observed,  $N_{\text{As}} \approx n_{77(0)} \approx n_{77i} \approx n_{77f}$  (curve 4).

Under arsenic activation annealing ( $350^\circ\text{C}$ ),  $\text{As}_2\text{Te}_3$  complexes decomposed, arsenic got incorporated in the Te sublattice as an acceptor, and the released tellurium nanocomplexes with typical concentration  $\sim 10^{17} \text{ cm}^{-3}$  were ready for reaction with  $\text{Hg}_l$  under IE. This is clearly seen from relaxation curves for activated samples with initial electron concentration  $n_{77i} \sim 10^{17} \text{ cm}^{-3}$ . If that is true, then *n*-type conductivity in as-grown samples was defined by the presence of  $\text{As}_2\text{Te}_3$  donor complexes, and not by  $\text{As}_{\text{Hg}}$  donors, which agrees with the results of Ref. [94].

### 3.3. Background donor concentration in $\text{HgCdTe}$

Fabricating high-quality *n*-type material is essential in MCT technology, as almost all types of MCT-based photodetectors use some kind of *n*-type material. *N*-type MCT can be fabricated using donor doping (mostly with indium or iodine), or just by relying on background donors. In high-grade MCT, they provide electron concentration of the order of  $10^{14}$ – $10^{15} \text{ cm}^{-3}$ , thus, it is important to know the exact value of this concentration for each MCT technology [96]. By background donor concentration ( $N_{BD}$ ), we understand here a total concentration of residual donor dopants and intrinsic donor defects. Extensive reviews on background impurities in MCT were given by Capper et al. [13,97]. As discussed above, the most important intrinsic donor defects in MCT is  $\text{Te}_{\text{Hg}}$ , especially for MBE-grown MCT [98].

The problem with establishing  $N_{BD}$  in MCT relates to the fact that detection limits of many physical and chemical methods, including SIMS (for many dopants  $> 10^{15} \text{ cm}^{-3}$ ), are much higher than doping levels of practical interest. This makes one try to establish  $N_{BD}$  with electrical measurements. In practice,  $N_{BD}$  is taken as electron concentration in *n*-type samples with low level of compensation when  $N_{BD} = n \ll n_i$ ,  $N_D - N_A$ . So, the measurements must be performed at low temperatures due to high  $n_i$ , which for MCT with  $x=0.2$  at  $300\text{ K}$  is  $\sim 4 \times 10^{16} \text{ cm}^{-3}$ , and for MCT with  $x=0.3$  is  $\sim 3 \times 10^{15} \text{ cm}^{-3}$ . To determine  $N_{BD}$  in *p*-type material, one needs to convert it into *n*-type and to minimize the electrical compensation. Low-temperature annealing in  $\text{Hg}$  vapor, which is used for *p*-to-*n* type CTC in vacancy-doped MCT, can only reduce  $[\text{V}_{\text{Hg}}]$  to a level corresponding to equilibrium with the vapor at a given temperature and cannot cope with residual acceptor impurities involved in the compensation effect. Annealing is also useless in application to *p*-to-*n* type CTC in MCT doped with I- and V-group acceptors. On the other hand, as discussed above, IE eliminates  $\text{V}_{\text{Hg}}$  almost completely [13], and also turns many residual acceptors (such as

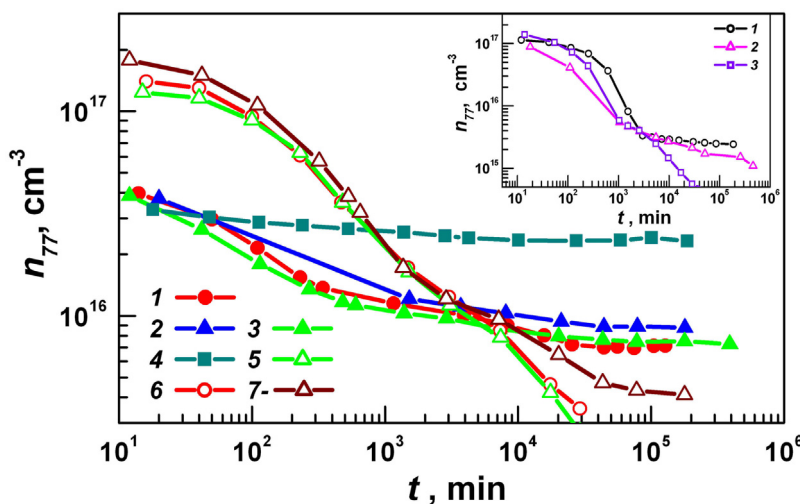


**Fig. 20.** Post-IE relaxation of the electron concentration in the modified (converted) 'bulk' n-layer for MBE-grown films: curves 1–4, as-grown n-type samples doped with As with cracking; 5–7, As-doped activated p-type samples. Inset shows relaxation for: curves 2 and 3, as-grown As-doped n-type samples with cracking at low cracking temperature, and, for comparison, in un-doped sample (curve 1).

As<sub>Te</sub>, Sb<sub>Te</sub>, Au<sub>Hg</sub>, Ag<sub>Hg</sub> and Cu<sub>Hg</sub>) into donors, whose concentration decreases upon storing the treated samples at the room temperature (see Sections 2.7 and 2.8). So, IE appears to be the only method useful for determining  $N_{BD}$  in extrinsically doped MCT [72,87].

In particular, in Refs. [50,72,87], when studying the effect of IE on the properties of MBE-grown n-MCT/GaAs ( $x_a \sim 0.22$ ), undoped and doped with In, it was proven that after short-term relaxation  $n_{77f}$  was determined by the sum of  $N_{BD}$  and concentration of introduced indium (Fig. 16). For the un-doped and weakly doped ( $N_{In} \sim 5 \times 10^{14} \text{ cm}^{-3}$ ) samples,  $n_{77f}$  equaled  $2.5 \times 10^{15} \text{ cm}^{-3}$ . Thus, in these samples  $n_{77f}$  appeared to much higher than  $n_{77(0)}$  and before IE the films were strongly compensated, with the compensation reduced by the etching. Also, in Ref. [72] it was shown that  $n_{77f}$  determined after short-time relaxation retained its value after 8 years of storage, which confirmed the stability of background doping in MCT. A similar effect was observed for As-doped MCT films, and in this case it was indicative of the fact that donor centers formed under IE between interstitial mercury and arsenic atoms indeed disintegrated via formation of neutral centers that were stable at 300 K. This allowed for determining  $N_{BD}$  in extrinsically acceptor-doped MCT. In particular, for As-doped MBE MCT/GaAs films with  $x_a = 0.22$  it was found that  $n_{77f} = N_{BD} = 2.5 \times 10^{15} \text{ cm}^{-3}$ , similar to the case of the un-doped samples (Fig. 10). As was shown in Ref. [87] (see Figs. 17 and 18), for all MBE-grown MCT/GaAs un-doped films with  $x = 0.2$   $N_{BD}$  equals  $(2\text{--}4) \times 10^{15} \text{ cm}^{-3}$  and does not depend on specific MBE technology. Electron concentration in MBE-grown MCT/GaAs films with  $x = 0.30$  after IE and short-term relaxation (Fig. 21) equaled  $(5\text{--}7) \times 10^{15} \text{ cm}^{-3}$  and appeared to be higher than that in the films with  $x \sim 0.2$  [87]. It was suggested that this fact was related to the higher substrate temperature used for the MBE growth of MCT with  $x \sim 0.3$  as related to the material with  $x \sim 0.2$ , as higher  $T_{sb}$  should lead to more intensive residual doping. The value of  $n_{77f}$  of  $(5\text{--}7) \times 10^{15} \text{ cm}^{-3}$  as typical of MCT with  $x \sim 0.3$  grown by MBE on GaAs substrates, remained stable for at least 7 years of storage at 300 K.

Long-term relaxation of electron concentration in nominally undoped MBE MCT films grown on Si substrates (MCT/Si) is presented in Fig. 22. Three pairs of films, with  $x_a = 0.29$ ,  $x_a = 0.25$  and  $x_a = 0.23$  were as-grown samples with n-type conductivity; three similar samples were annealed in helium atmosphere at  $T = 230\text{--}235^\circ\text{C}$  for 20 h to achieve p-type conductivity. As can be seen, in these samples, the electron concentration after short-term relaxation ( $2 \times 10^5 \text{ min}$ ) achieved the level of  $(2\text{--}4) \times 10^{14} \text{ cm}^{-3}$  and in some

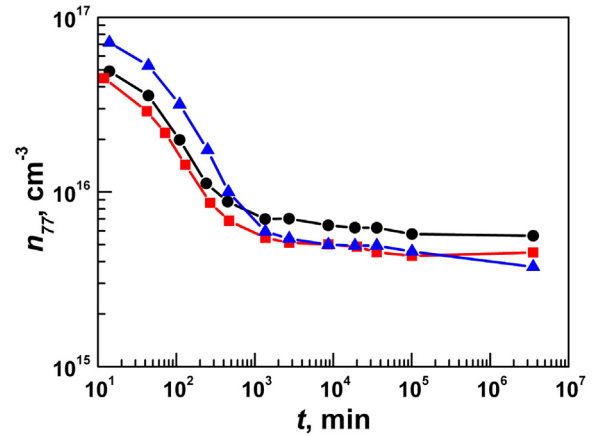


**Fig. 21.** Long-term post-IE relaxation of electron concentration in three similar MBE-grown MCT/GaAs films with  $x_a = 0.3$  (after [87]).

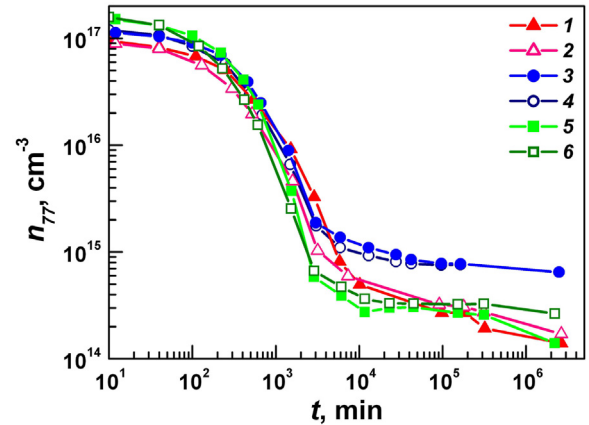


**Fig. 22.** Long-term post-IE relaxation of electron concentration in six MBE-grown MCT/Si films with  $x_a = 0.29$  (curves 1 and 2),  $x_a = 0.25$  (3 and 4) and  $x_a = 0.23$  (5 and 6), p- (1, 3 and 5) and n-type (2, 4 and 6) [52,87].

samples did not show tendency to level off and continued to decrease. Study of long-term stability of  $n_{77}$  confirmed this trend. Therefore, for MBE-grown MCT/Si films, the  $N_{BD}$  value appeared

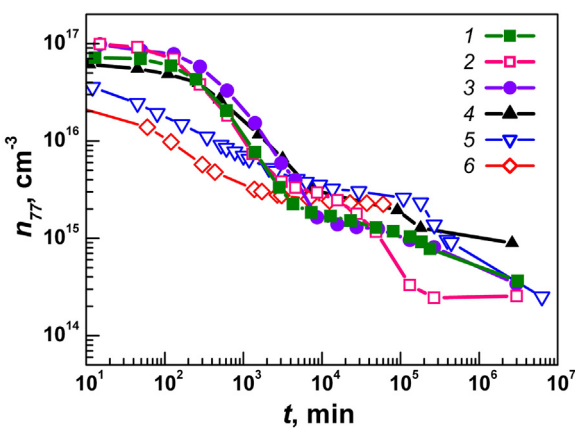


**Fig. 23.** Long-term post-IE relaxation of the electron concentration in the modified 'bulk' n-layer for LPE-grown films: curves 1 and 3,  $x_a \sim 0.20$ ; 4,  $x_a \sim 0.28$ , all three films were annealed into n-type; 2, 5 and 6, vacancy-doped p-type films with  $x_a \sim 0.20$ –0.23 [72,87].

to be one of order of magnitude lower than that for MCT/GaAs films, and did not depend on  $x$  (Fig. 18). According to the authors of Ref. [99], background doping in MBE-grown MCT is due to  $\text{Te}_{\text{Hg}}$ , and concentration of these defects depend on the growth temperature. However, comparison of  $N_{BD}$  in MCT/GaAs and MCT/Si (Figs. 16 and 22) grown at the same  $T_{sb} \sim 185^\circ\text{C}$  denounces this statement. It can be suggested that in MCT/GaAs the background doping is rather due to unintentional doping with Ga from the GaAs substrate.

For MCT grown with LPE,  $N_{BD}$  was found to be strongly dependent on the growth technology (Fig. 23). The samples whose relaxation is shown in Fig. 23 were grown at "Giredmet" (samples 1–4) [51] from the Te-rich melt on (111) $\text{Cd}_{0.96}\text{Zn}_{0.04}\text{Te}$  substrates and at JSC "Pure metals" (samples 5 and 6) [86]. In the latter case, the films were grown from the Te-rich melt on (111) $\text{CdTe}$  (sample 5) and (111) $\text{Cd}_{0.96}\text{Zn}_{0.04}\text{Te}$  (sample 6) substrates. The as-grown p-type films were annealed under mercury saturation to reduce  $[\text{V}_{\text{Hg}}]$  down to  $(5$ – $10) \times 10^{15} \text{ cm}^{-3}$  or for attaining n-type conductivity. In sample 6, which was grown at the stage when production of MCT met a number of challenges (*circa* 2003),  $n_{77f} = N_{BD}$  leveled off at  $\sim 2 \times 10^{15} \text{ cm}^{-3}$  straight after 5000 min of aging, which clearly indicated problems with the purity of the technology. In sample 5, which was grown at the climax of the development of the LPE technology (*circa* 1991), and in samples 1–4 from "Giredmet",  $n_{77f}$  after long-term relaxation reached  $2 \times 10^{14} \text{ cm}^{-3}$  with a clear tendency to decrease further.

Note that these data were specific to the material subjected to IE, and probably, some of the donor centers created by IE, continue to decompose for very long time. What happens to the defect structure further needed an additional study, which was difficult to perform because of the limitations of electrical measurements in relation to very low carrier concentrations.

From the practical point of view, summarizing the data for LPE- and MBE-grown materials, we can speak of a certain 'critical' value of  $N_{BD}$  in MCT irrelevant to growth technology and can set this value as  $10^{15} \text{ cm}^{-3}$ . If  $N_{BD}$  appears to be lower than that,  $n_{77f}$  will not stabilize after IE and it is necessary to perform donor doping to achieve stable and uniform parameters of the material used in the production of MCT-based photodetectors with the dry etching technology.

$N_{BD}$  for the bulk MCT was studied for material grown with vertical-directed crystallization with the replenishment from the solid phase at JSC "Pure Metals". IE-assisted studies of electrical properties of MCT crystals involved In-doped and crystals doped with Cu and Ag [79], and also Se (iso-valency dopant) [86]. Dop-

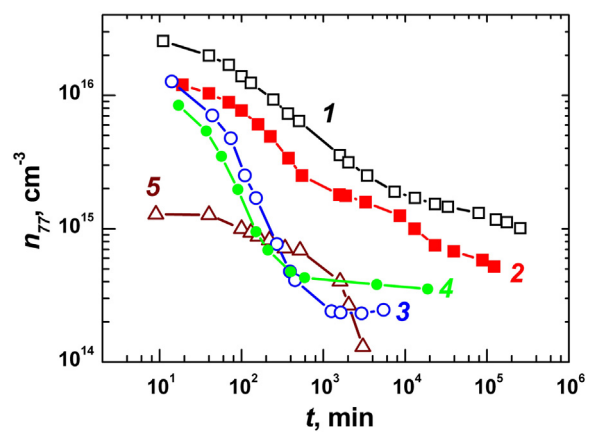


**Fig. 24.** Post-IE relaxation of the electron concentration in bulk MCT crystal: curves 1 and 2, In-doped ( $x=0.3$  and  $x=0.2$ , respectively); 3 and 4, doped with Ag or Cu; 5, doped with Se (after [87]).

ing with Se and In was performed from the melt with  $\sim 1\%$  Se and  $N_{\text{In}} \sim 5 \times 10^{14} \text{ cm}^{-3}$ . This type of low-level doping was used to 'stabilize'  $N_{BD}$  in the material. Doping with Cu and Ag was performed from the metallic films thermally evaporated on the crystal surface.

As can be seen in Fig. 24,  $n_{77f}$  values were very close in samples doped with Cu, Ag and In. This was explained by the fact that doping with acceptor impurities did not affect the  $N_{BD}$  value. For samples 1–4,  $N_{BD}$  could be estimated as  $(3$ – $10) \times 10^{14} \text{ cm}^{-3}$ , which definitely spoke of the high purity of the samples. Quite interesting result was obtained for samples doped with Se. After the relaxation, sample 5 with  $x=0.2$  showed very low  $n_{77f} \sim 1 \times 10^{14} \text{ cm}^{-3}$  with a tendency to subsequent relaxation that could not be traced due to the limitations of the discrete MSA procedure. To explain that, the authors had to consider that introducing Se (up to 2 at.%) in MCT stabilizes the weak Hg–Te bond, which makes the crystal more stable, but at the same time, reduces  $N_{BD}$  [87].

Thus, IE is an effective and a versatile tool for determining  $N_{BD}$  in MCT with both n- and p-type conductivity, including the material doped with acceptors. The value of  $N_{BD}$  in the majority of cases can be assessed after short-term relaxation of ion-etched samples at 300 K. IE allowed for establishing quite low  $N_{BD}$  in some MCT samples, of the order of  $10^{14} \text{ cm}^{-3}$ , and light donor doping is recommended to make sure that such samples have the correct value of resistivity and carrier concentration.

#### 4. Conclusion

The analysis performed in this review shows that the basic properties of MCT modified/converted with IE have been studied in much detail. Reliable quantitative models have been proposed for processes taking place during IE and after it, in the course of relaxation. All this allows for concluding that fabrication of p-n junctions for MCT-based photodiodes with the use of IE now has a solid physical basis and can be developed further. Despite a visible technological simplicity of IE as a method of photodiode fabrication as compared to ion implantation, it appears that the physical processes, which form the basis of conductivity type conversion, are quite complicated. As a method of photodiode fabrication, IE is less versatile than the implantation, as the former permits to form n-p-junctions only in initially p-type material, while ion implantation can be used for fabrication of both n-p and p-n junctions. Also, it looks like IE can be used for fabricating n<sup>+</sup>-n-p structures for photodiodes only in MCT with  $x \leq 0.4$ . Note, however, that thanks to considerable lateral extension of conductivity type conversion, IE allows for fabricating multi-element loop-hole photodiodes with

ring-type of *n-p* junction, which during hybridization with read-out circuits show excellent mechanical strength.

The analysis of the basic properties and features of modification of MCT with IE allows for proposing it as a new tool for studying defects in MCT. The use of IE allowed for revealing the presence, in MBE- and LPE-grown MCT, of specific neutral defects with the concentration of  $10^{17} \text{ cm}^{-3}$ , which probably are Te nanocomplexes. After IE and the relaxation the concentration of electrons in the basic volume of the converted (modified) *n*-layer is determined by the concentration of residual donors, and therefore IE is the most adequate method for determination of background donor concentration in MCT. Using of IE for the study of arsenic incorporation in MBE-grown MCT revealed specific mechanism of arsenic incorporation in MCT and provided better understanding of the requirements to arsenic doping in relation to fabrication of *p-n* heterostructures.

## Acknowledgments

The work at Tomsk State University was supported by The Tomsk State University D.I. Mendeleev Fund Program (research grant No 8.2.03.2017). The work at the Center for Microelectronics and Nanotechnology of the University of Rzeszow was partly supported by the authorities of the Podkarpackie Voivodeship (Marshall's Office of the Podkarpackie Voivodeship), contract WNDPPK.01.03.00-18-053/12.

## References

- [1] W.D. Lawson, S. Nielsen, E.H. Putley, A.S. Young, Preparation and properties of HgTe and mixed crystals of HgTe-CdTe, *J. Phys. Chem. Solids* 9 (1959) 325–329.
- [2] A.D. Shneider, I.V. Gavrilchak, Structure and properties of the HgTe-CdTe system, *Sov. Phys. Solid State* 2 (1960) 2079–2081.
- [3] A. Rogalski, Infrared Photodetectors, second edition, CRC Press, Boca Raton, 2011, pp. 876.
- [4] K. Fischer, Method of ion etching Cd-Hg-Te semiconductors, US Patent 4128467 (1978).
- [5] R.B. Withers, Method of manufacturing infrared detector elements, US Patent 4301591 (1979).
- [6] U. Solzbach, H.J. Richter, Sputter cleaning and dry oxidation of CdTe, HgTe and  $\text{Hg}_{1-x}\text{Cd}_x\text{Te}$  surface, *Surf. Sci.* 97 (1980) 191–195.
- [7] A.J. Stoltz, M. Jaime-Vasquez, J.D. Benson, J.B. Varesi, M. Martinka, Examination of the effect of high-density plasmas on surface of HgCdTe, *J. Electron. Mater.* 35 (2006) 1461–1464.
- [8] E.P.G. Smith, J.K. Gleason, L.T. Pham, E.A. Patten, M.S. Welkowsky, Inductively coupled plasma etching of HgCdTe, *J. Electron. Mater.* 32 (2003) 816–820.
- [9] E.P.G. Smith, G.M. Venzor, P.M. Goetz, J.B. Varesi, L.T. Pham, E.A. Patten, W.A. Radford, S.M. Jonson, A.J. Stoltz, J.D. Benson, J.H. Dinan, Scalability of dry-etch processing for small unit-cell HgCdTe focal-plane-arrays", *J. Electron. Mater.* 32 (2003) 821–826.
- [10] V. Srivastav, R. Pal, H.P. Vyas, Overview of etching technologies used for HgCdTe, *Opto-Electron. Rev.* 13 (2005) 197–211.
- [11] J.T.M. Wotherspoon, Methods of manufacturing a detector device, UK Patent GB 2095898 (1981).
- [12] V.I. Ivanov-Omskii, K.D. Mynbaev, Modification of  $\text{Hg}_{1-x}\text{Cd}_x\text{Te}$  properties by low-energy ions, *Semiconductors* 37 (2003) 1127–1150.
- [13] D. Shaw and P. Capper, "Conductivity Type Conversion", in "Mercury Cadmium Telluride: Growth, Properties and Applications", ed. by P. Capper, Wiley Series in Materials for Electronic and Optoelectronic Applications, P. Capper, S. Kasap, A. Willoughby, eds., (Chichester, J. Wiley & Sons, 2011), p. 297.
- [14] D. Shaw, P. Capper, The kinetics of conductivity type conversion in HgCdTe by ion beam milling, *J. Mater. Sci. Mater. Electron.* 19 (2008) 965–972.
- [15] I.I. Izhnin, S.A. Dvoretsky, N.N. Mikhailov, Yu.G. Sidorov, V.S. Varavin, K.D. Mynbaev, M. Pociask, Conductivity type conversion in ion-milled  $p\text{-Hg}_{1-x}\text{Cd}_x\text{Te}$ :As heterostructures grown by molecular beam epitaxy, *Appl. Phys. Lett.* 91 (2007) 132106.
- [16] P. Brogowski, H. Mucha, J. Piotrowski, Modification of mercury cadmium telluride, mercury manganese telluride, mercury zinc telluride by ion etching, *Phys. Status Solidi (a)* 114 (1989) K37–K40.
- [17] S. Rolland, R. Granger, R. Triboulet, *p-to-n* conversion in  $\text{Hg}_{1-x}\text{Zn}_x\text{Te}$  by ion beam milling effect, *J. Cryst. Growth* 117 (1992) 208–212.
- [18] N.N. Berchenko, V.V. Bogoboyashchiy, I.I. Izhnin, V.A. Yudenkov, Properties of *n*-layers formed by low energy ion beam milling of chalcogenides epitaxial films, *Phys. Status Solidi (c)* (2003) 872–874.
- [19] N.N. Berchenko, V.V. Bogoboyashchiy, I.I. Izhnin, M. Pociask, E.M. Sheregii, V.A. Yudenkov, Influence of the low energy ion beam milling on the electrical properties of InSb, *Phys. Status Solidi (c)* 2 (2005) 1418–1422.
- [20] A.V. Dvurechenskii, V.G. Remesnik, I.A. Ryazantsev, N.Kh. Talipov, Inversion of the conduction of  $\text{Cd}_x\text{Hg}_{1-x}\text{Te}$  films subjected to a plasma treatment, *Semiconductors* 27 (1993) 90–92.
- [21] M.V. Blackman, D.E. Charlton, M.D. Jenner, D.R. Purdy, J.T.M. Wotherspoon, C.T. Elliott, A.M. White, Type conversion in CdHgTe by ion beam treatment, *Electron. Lett.* 23 (1987) 978–979.
- [22] P. Brogowski, J. Rutkowski, J. Piotrowski, H. Mucha, Ion beam milling effect on surface properties of HgCdTe, *Electron. Technol.* 24 (1991) 93–96.
- [23] J.L. Elkind, Ion mill damage in *n*-HgCdTe, *J. Vac. Sci. Technol. B* 10 (1992) 1460–1465.
- [24] E. Belas, P. Höschl, R. Grill, J. Franc, P. Moravec, K. Lischka, H. Sitter, A. Toth, Deep *p-n* junction in  $\text{Hg}_{1-x}\text{Cd}_x\text{Te}$  created by ion milling, *Semicond. Sci. Technol.* 8 (1993) 1695–1699.
- [25] E. Belas, J. Franc, A. Toth, P. Moravec, R. Grill, H. Sitter, P. Höschl, Type conversion of *p*-(HgCd)Te using  $\text{H}_2/\text{CH}_4$  and Ar reactive ion etching, *Semicond. Sci. Technol.* 11 (1996) 1116–1120.
- [26] E. Belas, P. Höschl, R. Grill, J. Franc, P. Moravec, K. Lischka, H. Sitter, A. Toth, Ultrafast diffusion of Hg in  $\text{Hg}_{1-x}\text{Cd}_x\text{Te}$  ( $x \sim 0.21$ ), *J. Cryst. Growth* 138 (1994) 940–943.
- [27] E. Belas, R. Grill, J. Franc, A. Toth, P. Höschl, H. Sitter, P. Moravec, Determination of the migration energy of Hg interstitials in (HgCd)Te from ion milling experiments, *J. Cryst. Growth* 159 (1996) 1117–1122.
- [28] E. Belas, R. Grill, J. Franc, P. Moravec, R. Varghová, P. Höschl, H. Sitter, A.L. Toth, Dynamics of native point defects in  $\text{H}_2$  and Ar plasma-etched narrow gap (HgCd)Te, *J. Cryst. Growth* 224 (2001) 52–58.
- [29] G. Bahir, E. Finkman, Ion beam milling effect on electrical properties of HgCdTe, *J. Vac. Sci. Technol. A* 7 (1989) 348–353.
- [30] J.F. Siliquini, J.M. Dell, C.A. Musca, L. Faraone, Scanning laser microscopy of reactive ion etching induced *n*-type conversion in vacancy-doped *p*-type HgCdTe, *Appl. Phys. Lett.* 70 (1997) 3443–3445.
- [31] V.I. Ivanov-Omskii, K.E. Mironov, K.D. Mynbaev, Electrophysical properties of  $\text{Cd}_x\text{Hg}_{1-x}\text{Te}$  subjected to ion-beam treatment, *Sov. Phys. Semicond.* 24 (1990) 1379–1381.
- [32] V.I. Ivanov-Omskii, K.E. Mironov, K.D. Mynbaev,  $\text{Hg}_{1-x}\text{Cd}_x\text{Te}$  doping by ion-beam treatment, *Semicond. Sci. Technol.* 8 (1993) 634–637.
- [33] K.D. Mynbaev, N.L. Bazhenov, V.A. Smirnov, V.I. Ivanov-Omskii, Electrical properties of  $\text{Cd}_x\text{Hg}_{1-x}\text{Te}$  and  $\text{Zn}_x\text{Cd}_y\text{Hg}_{1-x-y}\text{Te}$  modified by low-energy ion bombardment, *Tech. Phys. Lett.* 28 (2002) 955–957.
- [34] I. Izhnin, V. Bogoboyashchiy, A. Kotkov, A. Moiseev, N. Grishnova, Type conductivity conversion in MOCVD  $\text{Cd}_x\text{Hg}_{1-x}\text{Te}/\text{GaAs}$  hetero-structures under ion milling, *Proc. SPIE* 5957 (2005) 595716.
- [35] R. Haakenaasen, T. Colin, H. Steen, L. Trodsdal-Iversen, Electron beam induced current study of ion beam milling type conversion in molecular beam epitaxy vacancy-doped  $\text{Cd}_x\text{Hg}_{1-x}\text{Te}$ , *J. Electron. Mater.* 29 (2000) 849–852.
- [36] R. Haakenaasen, T. Moen, T. Colin, H. Steen, L. Trodsdal-Iversen, Depth and lateral extension of ion milled *p-n* junctions in  $\text{Cd}_x\text{Hg}_{1-x}\text{Te}$  from electron beam induced current measurements, *J. Appl. Phys.* 91 (2002) 427–432.
- [37] V.V. Bogoboyashchiy, S.A. Dvoretsky, I.I. Izhnin, N.N. Mikhailov, Yu.G. Sidorov, F.F. Sizov, V.S. Varavin, V.A. Yudenkov, Properties of MBE  $\text{Cd}_x\text{Hg}_{1-x}\text{Te}/\text{GaAs}$  structures modified by ion-beam milling, *Phys. Status Solidi (c)* 1 (2004) 355–359.
- [38] D. Chandra, H.F. Schaake, F. Aqariden, T. Teherani, A. Kinch, P.D. Dreiske, D.F. Weirauch, H.D. Shih, *p* to *n* conversion in SWIR mercury cadmium telluride with ion milling, *J. Electron. Mater.* 35 (2006) 1470–1473.
- [39] D. Chandra, H.F. Schaake, M.A. Kinch, P.D. Dreiske, T. Teherani, F. Aqariden, D.F. Weirauch, H.D. Shih, Deactivation of arsenic as an acceptor by ion implantation and reactivation by low-temperature anneal, *J. Electron. Mater.* 34 (2005) 864–867.
- [40] V.V. Bogoboyashchiy, I.I. Izhnin, Mechanism for conversion of the type conductivity in *p*-Hg<sub>1-x</sub>Cd<sub>x</sub>Te crystals upon bombardment by low-energy ions, *Russ. Phys. J.* 43 (2000) 627–636.
- [41] V.V. Bogoboyashchiy, I.I. Izhnin, K.D. Mynbaev, The nature of compositional dependence of *p-n* junction depth in ion-milled *p*-Cd<sub>x</sub>Hg<sub>1-x</sub>Te, *Semicond. Sci. Technol.* 21 (2006) 116–123.
- [42] V.V. Bogoboyashchiy, A.I. Elizarov, V.I. Ivanov-Omskii, V.R. Petrenko, V.A. Petryakov, Kinetics of establishment of equilibrium between Cd<sub>x</sub>Hg<sub>1-x</sub>Te crystals and mercury vapour, *Sov. Phys. Semicond.* 19 (1985) 505–508.
- [43] D. Shaw, P. Capper, Conductivity type conversion in  $\text{Hg}_{1-x}\text{Cd}_x\text{Te}$ , *J. Mater. Sci. Mater. Electron.* 11 (2000) 169–177.
- [44] V.V. Bogoboyashchiy, I.I. Izhnin, Mechanism for creation of the mercury diffusion source at type conductivity conversion in *p*-Hg<sub>1-x</sub>Cd<sub>x</sub>Te under ion-beam milling, *Proc. SPIE* 5126 (2003) 427–433.
- [45] A. Sher, M.A. Berding, M. Van Schilfgaarde, A.B. Chen, HgCdTe status review with emphasis on correlations, native defects and diffusion, *Semicond. Sci. Technol.* 6 (1991) C59–C70.
- [46] C.M. Stahle, C.R. Helms, Ion sputter effects on HgTe, CdTe, and HgCdTe, *J. Vac. Sci. Technol. A* 10 (1992) 3239–3245.
- [47] V.V. Bogoboyashchiy, K.R. Kurbanov, Reaction constants for main cationic native defects in narrow-gap Hg<sub>1-x</sub>Cd<sub>x</sub>Te crystals, *J. Alloys Compd.* 371 (2004) 97–99.
- [48] E. Belas, R. Grill, J. Franc, H. Sitter, P. Moravec, P. Hoschl, A.L. Toth, Formation and propagation of *p-n* junction in *p*-(HgCd)Te caused by dry etching, *J. Electron. Mater.* 31 (2002) 738–742.

- [49] M. Pociask, I.I. Izhnin, S.A. Dvoretsky, Yu.G. Sidorov, V.S. Varavin, N.N. Mikhailov, N.H. Talipov, K.D. Mynbaev, A.V. Voitsekhovskii, Ion milling-induced conductivity-type conversion in p-type HgCdTe MBE-grown films with graded-gap surface layers, *Semicond. Sci. Technol.* 25 (2010) 065012.
- [50] M. Pociask, I.I. Izhnin, A.I. Izhnin, S.A. Dvoretsky, N.N. Mikhailov, Yu.G. Sidorov, V.S. Varavin, K.D. Mynbaev, Donor doping of HgCdTe for LWIR and MWIR structures fabricated with ion milling, *Semicond. Sci. Technol.* 24 (2009) 025031.
- [51] I.I. Izhnin, I.A. Denisov, N.A. Smirnova, M.M. Pociask, K.D. Mynbaev, Ion milling-assisted study of defect structure of HgCdTe layers grown by liquid phase epitaxy on CdZnTe substrates, *Opto-Electron. Rev.* 18 (2010) 328–331.
- [52] I.I. Izhnin, A.I. Izhnin, H.V. Savitskyy, M.M. Vakiv, Y.M. Stakhira, O.I. Fitsych, M.V. Yakushev, A.V. Sorochkin, I.V. Sabina, S.A. Dvoretsky, Yu.G. Sidorov, V.S. Varavin, M. Pociask-Bialy, K.D. Mynbaev, Defect structure of HgCdTe films grown by molecular-beam epitaxy on Si substrates, *Semicond. Sci. Technol.* 27 (2012) 035001.
- [53] J. Antoszewski, C.A. Musca, J.M. Dell, L. Faraone, Characterization of  $Hg_{0.7}Cd_{0.3}$ Te *n*-on-*p*-type structures obtained by reactive ion etching induced *p*-to-*n* conversion, *J. Electron. Mater.* 29 (2000) 837–840.
- [54] T. Nguen, J. Antoszewski, C.A. Musca, D.A. Redfern, J.M. Dell, L. Faraone, Transport properties of reactive-ion-etching-induced *p*-to-*n* type converted layers in HgCdTe, *J. Electron. Mater.* 31 (2002) 652–659.
- [55] G.P. Carey, S. Cole, T. Yamashita, J.A. Silberman, W.E. Spicer, J.A. Wilson, TEM investigation of the differences in ion milling induced damage of  $Hg_{1-x}Cd_x$ Te and CdTe heterojunctions, *J. Vac. Sci. Technol. A* 3 (1985) 255–258.
- [56] M.A. Lunn, P.S. Dobson, Ion beam milling of  $Cd_{0.2}Hg_{0.8}$ Te, *J. Cryst. Growth* 73 (1985) 379–384.
- [57] V. Savitsky, L. Mansurov, I. Podchuk, I.I. Izhnin, I. Virt, M. Lozynska, A. Evdokimenko, Peculiarities of MCT etching in RF mercury glow discharge, *Proc. SPIE* 3725 (1998) 299–303.
- [58] I.I. Izhnin, K.D. Mynbaev, M. Pociask, R.Ya. Mudryj, A.V. Voitsekhovskii, N.Kh. Talipov, Long-term room-temperature relaxation of the defects induced in  $(Hg,Cd)$ Te by low-energy ions, *Physica B* 404 (2009) 5025–5027.
- [59] M. Pociask, I.I. Izhnin, S.A. Dvoretsky, N.N. Mikhailov, Yu.G. Sidorov, V.S. Varavin, K.D. Mynbaev, V.I. Ivanov-Omskii, Electrical properties of *n*-HgCdTe heteroepitaxial layers modified by ion milling, *Semiconductors* 42 (2008) 1413–1415.
- [60] J.F. Siliquini, J.M. Dell, C.A. Musca, L. Faraone, J. Piotrowski, Characterisation of reactive-ion-etching-induced type-conversion in p-type HgCdTe using scanning laser microscopy, *J. Cryst. Growth* 184–185 (1998) 1219–1222.
- [61] J.F. Siliquini, J.M. Dell, C.A. Musca, E.P.G. Smith, L. Faraone, J. Piotrowski, Estimation of doping density in HgCdTe *p*-*n* junctions using scanning laser microscopy, *Appl. Phys. Lett.* 72 (1998) 52–54.
- [62] E.P.G. Smith, J.F. Siliquini, C.A. Musca, J. Antoszewski, J.M. Dell, L. Faraone, J. Piotrowski, Mercury annealing of reactive ion etching induced *p*-to-*n*-type conversion in extrinsically doped *p*-type HgCdTe, *J. Appl. Phys.* 83 (1998) 5555–5557.
- [63] K.D. Mynbaev, V.I. Ivanov-Omskii, Doping of epitaxial layers and heterostructures based on HgCdTe, *Semiconductors* 40 (2006) 1–21.
- [64] V.V. Bogoboyashchii, A.P. Vlasov, I.I. Izhnin, Mechanism for conversion of the conductivity type in arsenic-doped *p*- $Hg_{1-x}Cd_x$ Te subject to ionic etching, *Russ. Phys. J.* 44 (2001) 61–70.
- [65] N.N. Berchenko, V.V. Bogoboyashchii, I.I. Izhnin, A.P. Vlasov, Defect structure rebuilding by ion beam milling of As and Sb doped *p*- $Cd_xHg_{1-x}$ Te, *Phys. Status Solidi (b)* 229 (2002) 279–282.
- [66] N.N. Berchenko, V.V. Bogoboyashchii, A.P. Vlasov, I.I. Izhnin, Yu.S. Ilyina, Type conductivity conversion in As, Sb doped *p*- $Cd_xHg_{1-x}$ Te under ion beam milling, *Surf. Coat. Technol.* 158–159C (2002) 732–736.
- [67] V.V. Bogoboyashchii, I.I. Izhnin, K.D. Mynbaev, M. Pociask, A.P. Vlasov, Relaxation of electrical properties of *n*-type layers formed by ion milling in epitaxial HgCdTe doped with V-group acceptors, *Semicond. Sci. Technol.* 21 (2006) 1144–1149.
- [68] E. Belas, V.V. Bogoboyashchii, R. Grill, I.I. Izhnin, A.P. Vlasov, V.A. Yudenkov, Time relaxation of point defects in *p*- and *n*-(HgCd)Te after ion beam milling, *J. Electron. Mater.* 32 (2003) 698–702.
- [69] M. Pociask, I.I. Izhnin, S.A. Dvoretsky, N.N. Mikhailov, Yu.G. Sidorov, V.S. Varavin, K.D. Mynbaev, E. Sheregii, Ion milling-assisted study of defect structure of acceptor-doped HgCdTe heterostructures grown by molecular beam epitaxy, *Semicond. Sci. Technol.* 23 (2008) 095001.
- [70] I. Izhnin, S. Dvoretsky, N. Mikhailov, Yu. Sidorov, V. Varavin, M. Pociask, K. Mynbaev, R. Jakielo, G. Savitskyy, Arsenic incorporation in MBE-grown HgCdTe studied with the use of ion milling, *Phys. Status Solidi (c)* 7 (2010) 1618–1620.
- [71] I.I. Izhnin, S.A. Dvoretsky, K.D. Mynbaev, O.I. Fitsych, N.N. Mikhailov, V.S. Varavin, M. Pociask-Bialy, A.V. Voitsekhovskii, E. Szeregi, Defect study in molecular beam epitaxy-grown HgCdTe films with activated and unactivated arsenic, *J. Appl. Phys.* 115 (2014) 163501.
- [72] I.I. Izhnin, A.V. Voitsekhovskii, A.G. Korotaev, K.D. Mynbaev, V.S. Varavin, S.A. Dvoretsky, N.N. Mikhailov, M.V. Yakushev, A.Yu. Bonchyk, H.V. Savitskyy, E.I. Fitsych, Long-term stability of electron concentration in HgCdTe-based *p*-*n* junctions fabricated with ion etching, *Infrared Phys. Technol.* 73 (2015) 158–165.
- [73] I.I. Izhnin, H.V. Savitskyy, O.I. Fitsych, J. Piotrowski, K.D. Mynbaev, Electrical properties of HgCdTe films grown by MOCVD and doped with As, *Opto-Electron. Rev.* 21 (2013) 220–226.
- [74] N.N. Berchenko, V.V. Bogoboyashchii, I.I. Izhnin, K.R. Kurbanov, A.P. Vlasov, V.A. Yudenkov, Type conductivity conversion in *p*- $Cd_xHg_{1-x}$ Te, *Opto-Electron. Rev.* 11 (2003) 93–98.
- [75] M.A. Kinch, D. Chandra, H.F. Schaake, H.D. Shih, F. Aqariden, Arsenic-doped mid-wavelength infrared HgCdTe photodiodes, *J. Electron. Mater.* 33 (2004) 590–595.
- [76] I.M. Baker, C.D. Maxey, Summary of HgCdTe 2D array technology in the UK, *J. Electron. Mater.* 30 (2001) 682–689.
- [77] V.V. Bogoboyashchii, I.I. Izhnin, K.R. Kurbanov, Type of conductivity conversion in  $Cd_xHg_{1-x}$ Te single crystal doped with 1 group dopants under ion milling, *Appl. Phys. (2)* (2005) 48–53.
- [78] V.V. Bogoboyashchii, A.I. Elizarov, I.I. Izhnin, Conversion of conductivity type in Cu-doped  $Hg_{0.8}Cd_{0.2}$ Te crystals under ion beam milling, *Semicond. Sci. Technol.* 20 (2005) 726–732.
- [79] V.V. Bogoboyashchii, I.I. Izhnin, M. Pociask, K.D. Mynbaev, V.I. Ivanov-Omskii, Conductivity type conversion under ion milling of narrow-gap HgCdTe crystals doped with Au and Ag, *Semiconductors* 41 (2007) 804–809.
- [80] V.V. Bogoboyashchii, A.I. Elizarov, V.A. Petryakov, V.I. Stafeev, V.N. Severtsev, Investigation of copper diffusion in  $Cd_xHg_{1-x}$ Te single-crystals, *Sov. Phys. Semicond.* 21 (1987) 893–894.
- [81] K. Yang, Y.S. Lee, H.C. Lee, Annealing behavior of hydrogen-plasma-induced *n*-type HgCdTe, *Appl. Phys. Lett.* 87 (2005) 111905.
- [82] I.I. Izhnin, Temperature stability of the IBM formed  $Cd_xHg_{1-x}$ Te *p*-*n* structure, *Proc. SPIE* 3890 (1998) 519–522.
- [83] I.I. Izhnin, V.V. Bogoboyashchii, F.F. Sizov, Regularities of the  $Cd_xHg_{1-x}$ Te *p*-*n* junction formation by ion milling, *Proc. SPIE* 5957 (2005) 595713.
- [84] M. Pociask, I.I. Izhnin, K.D. Mynbaev, S.A. Dvoretsky, N.N. Mikhailov, Yu.G. Sidorov, V.S. Varavin, Blue-shift in photoluminescence of ion-milled HgCdTe films and relaxation of defects induced by the milling, *Thin Solid Films* 518 (2010) 3879–3881.
- [85] X. Zha, J. Shao, J. Jiang, W.Y. Yang, Blueshift in photoluminescence and photovoltaic spectroscopy of the ion-milling formed *n*-on-*p* HgCdTe photodiodes, *Appl. Phys. Lett.* 90 (2007) 201112.
- [86] I.I. Izhnin, V.V. Bogoboyashchii, F.F. Sizov, Electrical characteristics relaxation of ion milled MCT layers, *Proc. SPIE* 5881 (2005) 58810U.
- [87] I.I. Izhnin, K.D. Mynbaev, A.V. Voitsekhovsky, A.G. Korotaev, O.I. Fitsych, M. Pociask-Bialy, S.A. Dvoretsky, Background donor concentration in HgCdTe, *Opto-Electron. Rev.* 23 (2015) 200–207.
- [88] I.I. Izhnin, A.I. Izhnin, H.V. Savitskyy, O.I. Fitstch, N.N. Mikhailov, V.S. Varavin, S.A. Dvoretsky, Yu.G. Sidorov, K.D. Mynbaev, Defects in HgCdTe grown by molecular beam epitaxy on GaAs substrates, *Opto-Electron. Rev.* 20 (2012) 62–65.
- [89] I.I. Izhnin, K.D. Mynbaev, M.V. Yakushev, A.I. Izhnin, E.I. Fitsych, N.L. Bazhenov, A.V. Shilyaev, H.V. Savitskyy, R. Jakielo, A.V. Sorochkin, V.S. Varavin, S.A. Dvoretsky, Electrical and optical properties of CdHgTe films grown by molecular-beam epitaxy on silicon substrates, *Semiconductors* 46 (2012) 1341–1345.
- [90] M.M. Pociask, The study of HgCdTe MBE-grown structure with ion milling, *Opto-Electron. Rev.* 18 (2010) 338–341.
- [91] A.I. Belogorokhov, N.A. Smirnova, I.A. Denisov, L.I. Belogorokhova, B.N. Levonovich, Raman scattering in CdHgTe epitaxial layers grown on CdZnTe substrates, *Phys. Status Solidi (c)* 7 (2010) 1624–1626.
- [92] Z. Świątek, P. Ozga, I.I. Izhnin, E.I. Fitsych, A.V. Voitsekhovskii, A.G. Korotaev, K.D. Mynbaev, V.S. Varavin, S.A. Dvoretsky, N.N. Mikhailov, M.V. Yakushev, A.Yu. Bonchyk, H.V. Savitskyy, Electrical and optical studies of defect structure of HgCdTe films grown by molecular beam epitaxy, *Russ. Phys. J.* 59 (2016) 442–445.
- [93] J.W. Garland, C. Grein, S. Sivananthan, Arsenic *p*-doping of HgCdTe grown by molecular beam epitaxy (MBE): a solved problem? *J. Electron. Mater.* 42 (2013) 3331–3336.
- [94] P. Ballet, B. Polge, X. Biquard, I. Alliot, Extended X-ray absorption fine structure investigation of arsenic in HgCdTe: the effect of the activation anneal, *J. Electron. Mater.* 38 (2009) 1726–1732.
- [95] G.Yu. Sidorov, N.N. Mikhailov, V.S. Varavin, D.G. Ikusov, Yu.G. Sidorov, S.A. Dvoretskii, Effect of the arsenic cracking zone temperature on the efficiency of arsenic incorporation in CdHgTe films in molecular-beam epitaxy, *Semiconductors* 42 (2008) 651–654.
- [96] M. Kinch, The future of infrared; III-Vs or HgCdTe? *J. Electron. Mater.* 44 (2015) 2969–2976.
- [97] P. Capper, E.S. O'Keefe, C. Maxey, D. Dutton, P. Mackett, C. Butler, I. Gale, Matrix and impurity element distributions in CdHgTe (CMT) and (Cd,Zn)(Te,Se) compounds by chemical analysis, *J. Cryst. Growth* 161 (1996) 104–118.
- [98] V.S. Varavin, V.V. Vasiliev, S.A. Dvoretsky, N.N. Mikhailov, V.N. Ovsyuk, Yu.G. Sidorov, A.O. Suslyakov, M.V. Yakushev, A.L. Aseev, HgCdTe epilayers on GaAs: growth and devices, *Opto-Electron. Rev.* 11 (2003) 99–111.
- [99] V.S. Varavin, S.A. Dvoretsky, N.N. Mikhailov, Yu.G. Sidorov, Donor defects in epitaxial CdHgTe films grown with molecular-beam epitaxy method, *Avtometriya* (3) (2001) 9–19 (in Russian).